

AuraRing: Precise Electromagnetic Finger Tracking

FARSHID SALEMI PARIZI*, ERIC WHITMIRE*, and SHWETAK PATEL, University of Washington

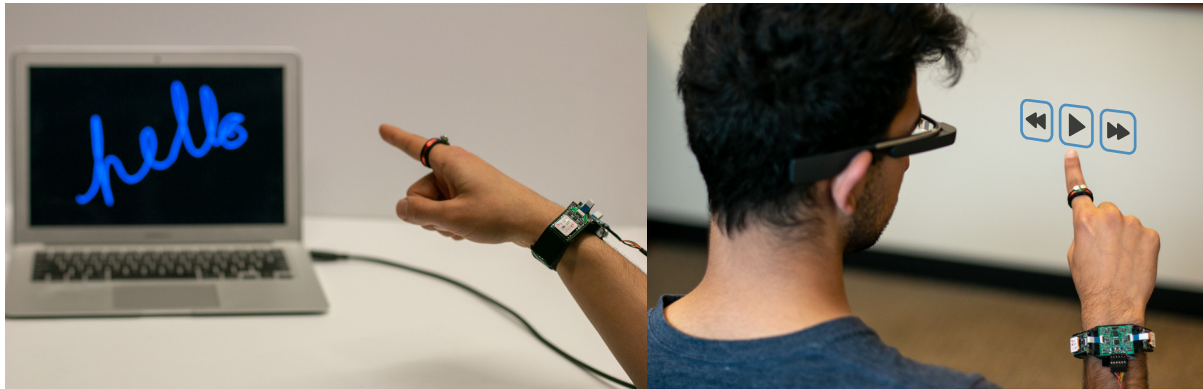


Fig. 1. AuraRing is 5-DoF electromagnetic tracker that enables precise, accurate, and fine-grained finger tracking for AR, VR and wearable applications. Left: A user writes the word "hello" in the air. Right: Using AuraRing to play a song in a music application on a smart glass.

Wearable computing platforms, such as smartwatches and head-mounted mixed reality displays, demand new input devices for high-fidelity interaction. We present AuraRing, a wearable magnetic tracking system designed for tracking fine-grained finger movement. The hardware consists of a ring with an embedded electromagnetic transmitter coil and a wristband with multiple sensor coils. By measuring the magnetic fields at different points around the wrist, AuraRing estimates the five degree-of-freedom pose of the ring. We develop two different approaches to pose reconstruction—a first-principles iterative approach and a closed-form neural network approach. Notably, AuraRing requires no runtime supervised training, ensuring user and session independence. AuraRing has a resolution of 0.1 mm and a dynamic accuracy of 4.4 mm, as measured through a user evaluation with optical ground truth. The ring is completely self-contained and consumes just 2.3 mW of power.

CCS Concepts: • **Human-centered computing** → **Interaction devices**; **Ubiquitous and mobile computing**.

Additional Key Words and Phrases: Electromagnetic tracking, mixed reality, wearable, input, finger tracking

ACM Reference Format:

Farshid Salemi Parizi, Eric Whitmire, and Shwetak Patel. 2019. AuraRing: Precise Electromagnetic Finger Tracking. *Proc. ACM Interact. Mob. Wearable Ubiquitous Technol.* 3, 4, Article 150 (December 2019), 28 pages. <https://doi.org/10.1145/3369831>

*Both authors contributed equally to this research.

Authors' address: Farshid Salemi Parizi, farshid@cs.washington.edu; Eric Whitmire, emwhit@cs.washington.edu; Shwetak Patel, shwetak@cs.washington.edu, University of Washington, Seattle, WA.

Permission to make digital or hard copies of all or part of this work for personal or classroom use is granted without fee provided that copies are not made or distributed for profit or commercial advantage and that copies bear this notice and the full citation on the first page. Copyrights for components of this work owned by others than the author(s) must be honored. Abstracting with credit is permitted. To copy otherwise, or republish, or post on servers or to redistribute to lists, requires prior specific permission and/or a fee. Request permissions from permissions@acm.org.

© 2019 Copyright held by the owner/author(s). Publication rights licensed to ACM.

2474-9567/2019/12-ART150 \$15.00

<https://doi.org/10.1145/3369831>

Proc. ACM Interact. Mob. Wearable Ubiquitous Technol., Vol. 3, No. 4, Article 150. Publication date: December 2019.

1 INTRODUCTION

New computing platforms are becoming increasingly coupled to the user. Wearable devices like smartwatches, smart rings, and head-mounted mixed reality devices are offering unprecedented access to computing and information on the go. As computing platforms evolve from devices we carry with us to devices we wear on us, there is a renewed demand for input techniques that are decoupled from the display. These input devices must be continuously available and subtle to support various contexts of use while enabling robust and expressive interaction.

Many of today’s most effective input devices rely on continuous tracking of the fingers or handheld objects; smartphones and smartwatches track 2D finger position, a mouse tracks 2D hand position, and augmented reality devices like the Microsoft HoloLens 2 track the 3D pose of the finger. These proven input techniques stand in contrast to existing lines of research around sensor-based efforts to track finger motion, which often focus on discrete, gesture-based interactions [4, 14, 44, 52, 62]. Although gesture recognition is useful, it is just one part of the interaction language needed for mobile wearable computing. For common tasks like object manipulation, drawing, sliding, swipe-based text input, or body-pose reconstruction, an input device that supports absolute, continuous tracking with millimeter-level precision will be most appropriate. Moreover, building a gesture recognizer on top of a tracking system, instead of direct classification from a sensor stream, can enable input devices that are more robust and extensible (e.g. supporting different users and contexts out of the box).

In this work, we present AuraRing, a precise, millimeter-level ring tracking system. AuraRing consists of two components: a wireless, self-contained ring and a wristband that tracks the absolute position and orientation of the ring with respect to the wristband in real-time. The low-power, battery-operated ring generates an oscillating magnetic field around the hand. As the user moves their finger and wrist, the relative position and orientation of this field changes with respect to the wristband. Sensors embedded in the wristband measure these fields at different locations and use these measurements to estimate the pose of the ring with respect to the wristband. AuraRing is effectively a 5 degree-of-freedom (DoF) tracking system—that is, it tracks three positional components (x , y , z) and two rotational components (yaw and pitch) of pose. When the ring is worn, this allows AuraRing to capture flexion/extension and abduction/adduction of both the wrist and finger metacarpal joint. Although the ring can be worn on any finger, we envision most users would wear it on the index finger for maximum dexterity.

Compared to prior work, our approach leverages common device form-factors—a wristband and a ring—and does not require affixing magnets [6, 7, 16, 19], iron-core coils [8], or magnetometers [6, 7, 19] to the fingertips. AuraRing leverages the insight that an electromagnetic coil is better placed around the finger than on it. Our approach also delivers significant improvements in power, range, portability, and tracking precision.

Electromagnetic tracking has a long history of use in meter-scale tracking applications [29, 37, 38, 41, 46, 47] in a variety of domains. Though precise, electromagnetic tracking has a reputation for being power-hungry and subject to environmental interference. AuraRing overcomes these challenges by explicitly focusing on short-range (10 cm to 15 cm) tracking. This range reduces the scope of possible interfering objects and allows the AuraRing transmitter to use approximately 2000x less power than a typical commercial EM tracking system [41]. Unlike existing electromagnetic tracking systems that use a three-axis transmitter and a three-axis receiver, AuraRing uses a single transmitter coil wrapped around a ring and multiple three-axis sensors around a wristband. This enables a form-factor suitable for wearable use. Compared to other sensing modalities like radio frequency, infrared, optical, and inertial sensing, electromagnetic tracking offers an avenue for absolute positional tracking without drift issues or the need for compute, sensing, or active communication on the ring itself.

Because AuraRing leverages physics models, it works out of the box after a one-time factory calibration with ground-truth tracking data from a motion-capture system. By grounding the calibration model in physics, we significantly simplify the number of parameters that need to be learned for a complete simulation of the device. We present two tracking solutions that leverage this model — a optimization-based approach and a neural network

approach trained only on simulated data. We demonstrate that at runtime, AuraRing can track finger motion across different users despite small changes in how the device is positioned on the wrist and finger.

AuraRing offers a flexible solution for tracking the finger in either direct or indirect pointing tasks. We envision that AuraRing can be used either as a standalone input device, or in tandem with a wrist-tracking solution. For standalone scenarios, AuraRing offers a rich input source for smartwatches or smart glasses. With AuraRing, a user can provide input using their finger and wrist while keeping their arm motionless at their side or resting on a table. This capability is particularly useful in public settings, when large hand motions would be distracting and socially unacceptable.

AuraRing can also be used to track the absolute position of the finger in head-space with respect to the user's vision. In mixed-reality scenarios, precise hand and finger tracking enables many compelling applications. For example, buttons, sliders, and interactive widgets can be placed in the air, on environmental surfaces, or on the body. AuraRing can be operated in concert with a head-mounted camera that tracks the wrist with respect to the head using fiducials on the wristband.

Our primary contributions include:

- (1) A hardware architecture for a one-axis transmitter ring and multi-sensor wristband that enables low-power finger tracking in a compact form-factor.
- (2) Two tracking algorithms, including a physics-based iterative approach and a closed-form neural network approach to 5-DoF pose estimation.
- (3) A system characterization and user evaluation demonstrating a sensor resolution of 100 μm and dynamic tracking accuracy of 4.4 mm on a session-independent task.

2 RELATED WORK

2.1 Magnetic Tracking

Magnetic tracking systems can be characterized by whether they use direct current (DC) or alternating current (AC) to produce magnetic fields. In DC tracking systems, a magnetic sensor, often a magnetometer, measures the magnetic field generated by an electromagnet or permanent magnet. This technique has seen extensive use in the HCI community, since magnetometers are commonly found in wearable devices and permanent magnets can be easily attached to the body. Abracadabra [16] and McIntosh [33] used permanent magnets affixed to the fingertip to interact with a smartwatch that measures the magnetic field direction and strength using magnetometers. Similarly, uTrack [7], affixed a permanent magnet to the thumb and two magnetometers to the fingers to track 3D thumb pose. FingerPad [6] also affixes a magnet to thumb but uses a Hall-effect sensor grid on the index fingernail to sense pinch gestures. The Nanya system [4] used a ring with two permanent magnets attached that could be twisted to change the shape of the resulting magnetic fields, which were measured by a magnetometer on a smartwatch. In 2016, Lyons showed a smartphone-based magnetometer tracking system that enabled 2D interaction on the side of a cardboard VR device using a permanent magnet [32]. Reyes et al demonstrated SynchroWatch [44], which recognizes synchronous thumb gestures using a permanent magnet attached to a thumb ring. Magnetic tracking systems that rely on permanent magnets have size and complexity advantages because they can rely on off-the-shelf magnets and magnetometers. However, this comes at the cost of precision. Magnetometers are generally limited in their accuracy and sampling rate and such systems must contend with interference from the Earth's geomagnetic field. As a result, the operating range of such systems is generally limited to several centimeters.

In contrast, AC magnetic tracking relies on one or more oscillating magnetic fields. AC electromagnetic tracking has a rich history of enabling precise, 6-DoF tracking [29, 43]. Since its inception in the late 1970's, the technique has been used for surgical tracking [9, 30, 56], biomechanical analysis [34, 39], virtual reality tracking [26, 54, 55], and HCI [8, 20, 40]. A typical electromagnetic tracking system contains a transmitter base station with a three-axis

orthogonal coil transmitter and one or more three-axis receivers, typically realized using orthogonal coils. The oscillating magnetic flux through the coils induces an oscillating voltage of the same frequency, which can be amplified and measured. Filtering or synchronous detection is used to isolate the field of interest from other ambient magnetic fields, including the geomagnetic field. Original systems relied on iterative approaches to estimate the pose of the tracked objects. However, recent techniques have explored closed-form or closed-loop solutions that improve performance [12, 26]. Magnetic field distortions when tracking near metallic objects is a common drawback of AC magnetic tracking, particularly when used in dynamic environments. Some work has attempted to account for magnetic interference through a secondary calibration step [27, 28]. See the work by Pasku et al for a more thorough review of magnetic tracking systems [38].

In addition to research advances, there are several commercial AC magnetic tracking solutions on the market. Systems from Polhemus [41] and NDI [37] offer sub-millimeter tracking accuracy at a range of dozens of centimeters. Both the Razer Hydra and the Magic Leap One use electromagnetic tracking for handheld controllers.

AuraRing relies on short-range AC electromagnetic tracking to achieve precise tracking of a ring from a wristband. Unlike permanent magnet-based approaches, AuraRing is not susceptible to interference from the Earth's geomagnetic field and the use of AC current significantly improves the tracking precision. Because AuraRing operates at distances on the order of 10 cm and relies on resonant coils pairs, it consumes significantly less power than commercial AC electromagnetic tracking devices, which often use several watts of power. In contrast, AuraRing consumes orders of magnitude less power (2.3 mW vs 5 W [41]), making it suitable for use as a wearable device. The short range also significantly reduces the impact of interference from nearby metallic objects. Another key architectural difference between AuraRing and other AC magnetic tracking systems is the use of a single transmitter axis. This design choice allows minimal hardware on the transmitter ring at the cost of additional sensors on the wristband.

Conceptually, AuraRing is most similar to Finexus [8]. Unlike Finexus, which had a range limited to a few centimeters and used high-power, wired electromagnets affixed to the fingertips, AuraRing has a unique form factor that embeds the electromagnetic transmitter into a ring. The low power consumption allows the ring to be self-powered. Additionally, while Finexus used four magnetometers, AuraRing uses three coil-based sensors, which have a much higher bandwidth, enabling better temporal smoothing and detection of high frequency impact events.

2.2 Other Approaches for Finger Tracking

Beyond magnetic tracking approaches, researchers have leveraged other sensing techniques to estimate fine-grained finger motion. Kim et al used infrared illumination from the wrist to track hand pose [25]. Although this method can enable full hand tracking, the form factor limits practicality. Project Soli [52] uses radio frequency signals to recognize subtle finger gestures. Pyro uses the pyroelectric effect to recognize small thumb gestures [14]. Bioimpedance has been used to reconstruct the cross-sectional impedance of the arm and recognize various hand gestures [62, 63]. There has been also work in using capacitive sensing [50] and ultrasound [21] for discrete hand gesture recognition from a wristband. These methods result in discrete, gesture-based interactions and not continuous tracking.

Other systems use sensors on the opposing arm or in the environment to track finger motion. FingerIO uses sonar from a smartphone to measure the 2D position of the fingertip [36]. SkinTrack uses a ring-smartwatch pair that leverages electrical waveguides to track the 2D position of the finger on the opposing arm [64]. Our AuraRing device uses a similar form-factor, but enables 5-DoF tracking of the finger in free space. Another approach is the use of gloves or finger strips to estimate finger and hand pose [1, 3, 13, 18, 19, 48, 53, 60, 61]. These systems require significant augmentation and are less appropriate for everyday usage.

Finally, camera-based approaches are a common approach to hand- and finger- tracking. These commonly rely on infrared depth sensing [49] or markers on the hand [51]. Unique placements of the cameras have led to interactive systems that offer subtle input [5, 25, 31].

2.3 Smart Rings

Smart rings provide an attractive form-factor for always-available subtle input. Rings have been shown useful for subtle input [4, 59], interaction with 2D surfaces [24, 35, 58], haptic feedback [23, 45], and text-entry for wearable computing [10, 11, 15]. LightRing [24] and Magic Finger [58] is most similar to AuraRing in its goals and uses a gyroscope and IR proximity sensor and optical mouse sensor respectively to track finger motion on a 2D surface. However, by moving the sensing components from the ring to the wrist, AuraRing can use a slimmer ring design with minimal power consumption. AuraRing also differs in that it tracks the absolute 5-DoF pose of the finger and can be used for more than just 2D input on a surface. Commercial smart rings offer features like fitness tracking, heart-rate tracking, inertial gesture sensing, and NFC payments. Inertial sensing on a ring has the potential to track wrist and finger motion, though it is subject to drift and recalibration issues. Moreover, inertial tracking of the finger would require significant data transmission between the ring and the processing unit, leading to either high power consumption or unwieldy cables [15, 59]. Commercial smart rings that feature IMU gesture recognition are not streaming continuous sensor data, but are more likely to process data on-device and send a message over Bluetooth whenever a specific gesture is detected. This limits these devices to detecting specific gestures. In contrast, AuraRing can transmit all the time using only 2.3 mW, which we show enables continuous high-speed ring tracking without the need for additional RF communication.

3 THEORY OF OPERATION

3.1 AuraRing Physics

Magnetic tracking is generally realized either with magnetometers to track a permanent magnet [4, 7, 19] or with inductive coils to track an alternating current (AC) electromagnet [29, 37, 41, 43, 46, 47, 54–56]. Static magnetic fields created by a permanent magnet are inseparable from the Earth’s geomagnetic field—an effect which becomes critical when operating at distances beyond a few centimeters. To isolate the signal of interest, AuraRing uses AC electromagnetic coils to generate a magnetic field at a particular frequency (32 kHz). Maxwell’s equations state that an AC magnetic field is generated when an AC electric current is passed through a wire coil. As depicted in Figure 2, AuraRing uses a wire coil wrapped around the ring to produce an oscillating magnetic field around the hand. According to Faraday’s law, a voltage is induced in the other sensor coils in the presence of this oscillating magnetic field. The induced voltage is proportional to rate of change of magnetic flux through the sensor coil, which will change as a function of the position and orientation of the sensor coils with respect to the transmitter coil. More specifically, if the sensor coil is aligned with the field (i.e., the normal vector to the coil is aligned with the field), then the magnitude of the induced voltage will be maximized. As the coil rotates away from the field, the induced voltage decreases to zero. If the coil continues to rotate even further, the voltage acquires a 180° phase shift that manifests as a negative amplitude.

Traditional 6-DoF electromagnetic trackers use a 3-axis transmitter and a 3-axis sensor coil, which is difficult to achieve in a ring form-factor where size and battery life are paramount. However, a ring is a convenient form-factor for a single-axis air core coil that wraps around the finger. Using a single-axis coil makes the entire system insensitive to changes in the roll of the transmitter along the magnetic axis; conveniently, such movement is not physically possible in finger-tracking scenarios. To compensate for the lack of three transmitter axes, AuraRing leverages three 3-axis sensor coils embedded at known locations within a wristband. By measuring the magnetic fields at different points in space, AuraRing reconstructs the 3-DoF position and 2-DoF orientation of

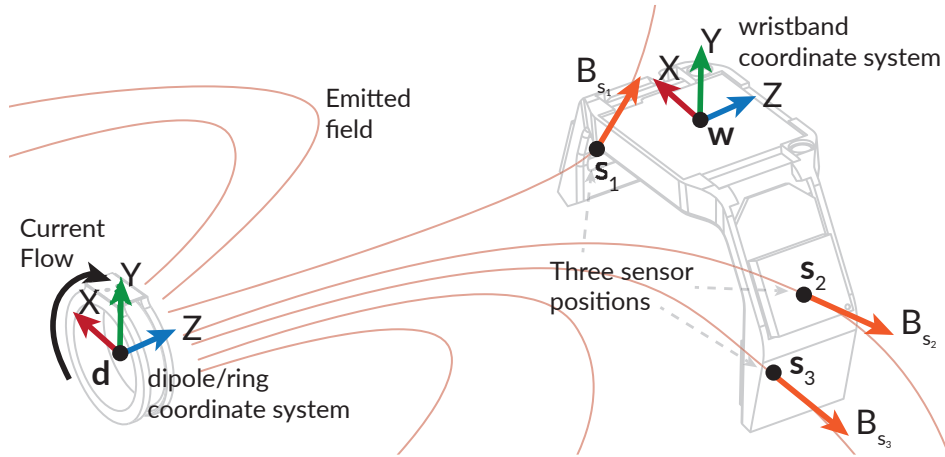


Fig. 2. AuraRing uses a wire coil wrapped on a ring to produce an AC magnetic field around the hand which is measured by three 3-axis coils embedded in a wristband.

the ring. Figure 2 illustrates the configuration of the AuraRing transmitter and sensors as well as the coordinate systems used throughout this paper.

3.2 Magnetic Field Model

We construct a physics-based simulation to model the behavior of our system under different configurations, such as changing the number or placement of sensor coils. Because the ring diameter is much smaller compared to the distance between the ring and wristband, we use standard magnetic field equations to model the ring as a dipole emitter. This magnetic field model represents the inverse of the tracking problem — it estimates the magnetic fields given the ring position, whereas the tracking problem seeks to estimate the ring position given measurements of the magnetic field. This is useful for simulation and it also forms the basis of the optimization-based tracking algorithm discussed in section 6.1. In this paper, we adopt the notation ${}^A\mathbf{v}$ to represent the \mathbf{v} vector in the A coordinate frame. The notation ${}^B\mathbf{R}$ represents a rotation transformation from the A to B coordinate frame. In practice, these transforms are implemented using quaternion algebra, but other representations would be appropriate as well.

The model seeks to estimate the magnetic field vector measured at each sensor coil, s_i , where s_i indicates the sensor coil of interest. Because the transmitter is embedded within the object to be tracked, we first conduct a series of coordinate system transformations to reduce the model to simple dipole analysis with known closed-form solutions. Let d be the dipole coordinate frame with the magnetic axis oriented in the z -direction, that is, in a direction along the finger (see Figure 2). This is coincident with the ring coordinate frame. Let w be the wristband coordinate frame, which contains multiple sensors, s_i , at positions ${}^w\mathbf{s}_i$ and orientations ${}^s_i\mathbf{R}$, as depicted in Figure 2. These transforms are defined in the wristband coordinate frame and are known from the 3D geometry of the wristband enclosure and electronics.

Given any possible position of the dipole/ring with respect to the wristband (${}^w\mathbf{d}$), and the geometry of the sensors (${}^w\mathbf{s}_i$), we first compute the position of the sensor in the dipole frame:

$${}^d\mathbf{s}_i = {}^d_w\mathbf{R} ({}^w\mathbf{s}_i - {}^w\mathbf{d}) \quad (1)$$

We can decompose this sensor position vector, ${}^d\mathbf{s}_i$, into x , y , and z components (see Figure 2) and compute the distance between the dipole and sensor, $r = |{}^d\mathbf{s}_i| = \sqrt{x^2 + y^2 + z^2}$. We then use standard the magnetic dipole equation derived from the Biot-Savart law under quasistatic assumptions to compute the expected magnetic field at each sensor location (${}^d\mathbf{B}_{s_i}$). This equation captures the magnetic field at any point around a standard dipole. Note that we omit the magnetic dipole constants here for brevity and because we are only interested in the relative field strengths.

$${}^d\mathbf{B}_{s_i} = \left\langle \frac{3xz}{r^5}, \frac{3yz}{r^5}, \frac{3z^2 - r^2}{r^5} \right\rangle \quad (2)$$

This gives us the magnetic field vectors at each sensor in the ring/dipole coordinate frame. To estimate what each sensor would measure, we rotate once more to compute this magnetic field in the sensor frame of reference:

$${}^s\mathbf{B}_{s_i} = {}^s\mathbf{R}_w {}^d\mathbf{R}_w^T ({}^d\mathbf{B}_{s_i}) \quad (3)$$

3.3 Number of Sensors Required

To inform the design of AuraRing, we conducted a preliminary analysis using this model in which we varied the number of sensor coils. Choosing a sensor coil configuration requires balancing performance versus size and power. Tracking the ring is at least a 4-DoF problem, since both the wrist and finger metacarpal joints have two degrees of freedom. As a result, a robust approach requires at minimum two coils; each coil measures a three-dimensional field vector from a single emitter, so two coils would provide six sensor values. In practice, due to the potential for small shifts of the band on the wrist, AuraRing tracks as a 5-DoF problem (x , y , z , pitch, yaw), which we hypothesized might be difficult with just two sensor coils. A configuration is considered robust if, for a set of observed sensor values, there is a unique position and orientation within reasonable bounds that explain those observations.

To explore the design space of coils, we first choose a test point, representative of a typical ring position and orientation, and use the physics model described previously to compute the magnetic field as observed from each sensor. We then compare this observation of magnetic field vectors to what one would observe if the ring were at any other position and orientation. In a robust design, no other position or orientation would produce a similar observation. We select a dense sampling of possible ring positions and orientations within the tracking bounds for comparison. The x , y , and z axes are defined according to the wristband frame in Figure 2, with the finger generally pointing along the $-Z$ axis. For possible positions, we sample at 2 mm intervals within the bounds of $-40 \text{ mm} < x < 40 \text{ mm}$, $-130 \text{ mm} < y < 80 \text{ mm}$, and $-140 \text{ mm} < z < -50 \text{ mm}$. For orientation, we define θ as pitch (in the extension/flexion direction) and ϕ as yaw (in the adduction/abduction direction). We use these Euler angles to generate a quaternion orientation at 2° intervals within the bounds $-90^\circ < \theta < 90^\circ$ and $-60^\circ < \phi < 60^\circ$. These bounds correspond to typical bounds of the ring after simulation of finger kinematics with measurements taken from a representative hand.

Figure 3 illustrates an example result of this analysis for a single target point. The points in each plot indicate locations that can produce a set of sensor measurements similar to that produced at the target point under any tested rotation. This means that for a given point in the plot, there is some ring orientation at that position that could be confused for the target point, shown in red. The color indicates the measure of similarity to the target point.

As expected for a device with only a single sensor, there is a large confusion volume along all dimensions. Interestingly, there is a defined minimum for a 2-sensor setup, but the problem is ill-conditioned along some directions. This suggests that a 2-sensor device might suffice with the proper constraints, but any noise could result in significant errors. The 3-sensor setup produces a well-conditioned minimum, justifying our use of

three coils around the wristband. Although this particular example does not reveal much about optimal sensor placements, robustness is maximized when the sensor coils placements are maximally spread apart.

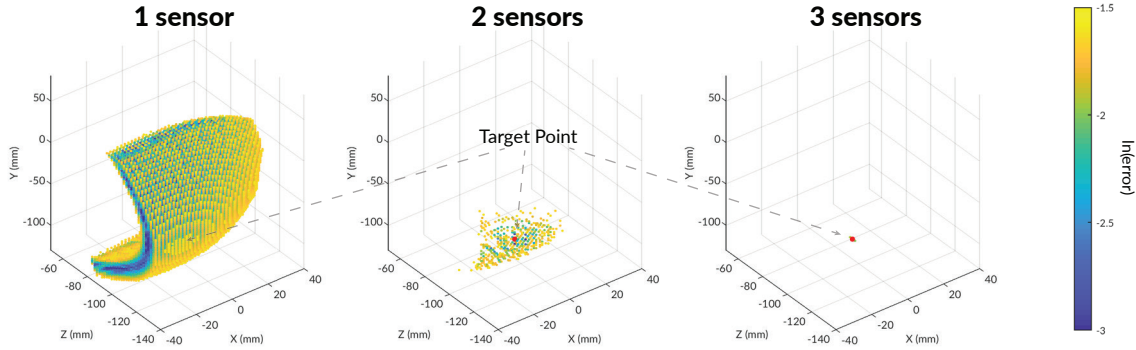


Fig. 3. By embedding three sensor coils in the wristband, AuraRing achieves a well-conditioned minimum that makes AuraRing robust. As depicted, having one or two coils will result in confusing other points with the target point.

4 AURARING HARDWARE

The AuraRing system consists of a ring that generates an AC magnetic field and a wristband with three embedded sensors that measure the resulting fields. Figure 4 depicts the AuraRing system components and Figure 5 shows a close up of the electronics on the wristband. The following sections describes the AuraRing hardware, explores the hardware’s capabilities, and enumerates design challenges.

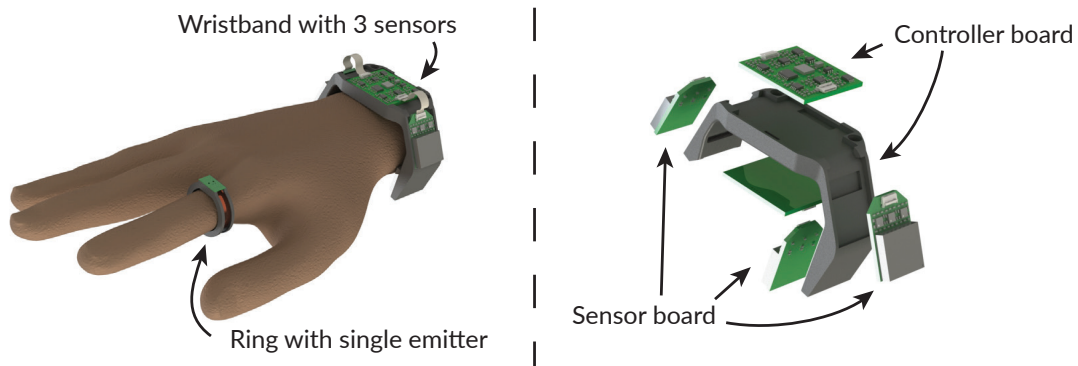


Fig. 4. AuraRing contains two controller and three sensor boards embedded in a wristband and a ring worn device.

4.1 Ring

In designing AuraRing, we pursued a design that would resemble device form-factors that users are already accustomed to in order to present a plausible path forward for everyday use. For the ring-based transmitter, rather

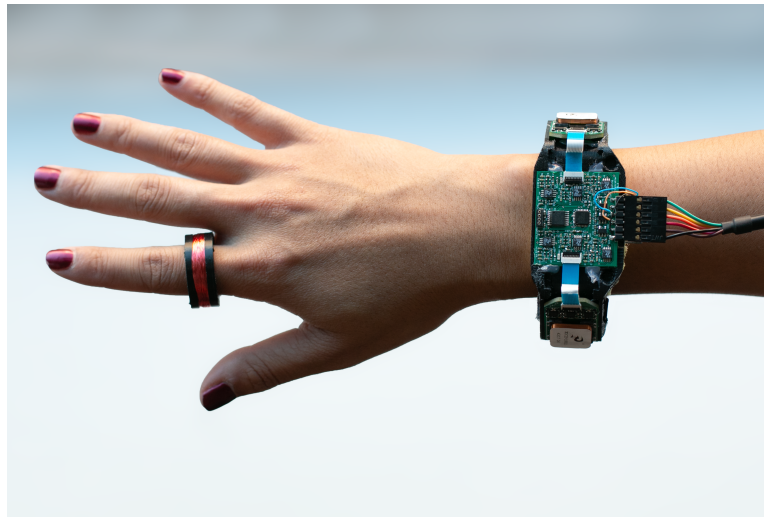


Fig. 5. Close up of AuraRing hardware

than affixing an iron-core coil [8] or permanent magnet [6, 7] to the top of the finger, we designed a custom electromagnet transmitter compatible with a ring form-factor. In doing so, we were forced to put minimal digital electronics on the ring to ensure a slim form-factor and minimize power consumption. AuraRing's ring consists of a single-axis low-profile transmitter coil that emits a magnetic field oscillating at 32.768 kHz. The transmitter coil consists of 600 turns of 42 AWG magnet wire wound around a 3D-printed ABS ring with a diameter of 20 mm. The inductance of the coil is approximately 15 mH. In general, the field strength will increase with the number of turns, but other factors like the DC resistance, capacitance, the skin effect [42] can degrade performance if too many turns of thin wire are used. The number of turns and wire gauge was chosen through a combination of electrical simulation and experimentation in order to maximize signal-to-noise ratio without the need for additional amplification. The actual diameter of the ring can be chosen to fit a particular user's finger size, much like today's commercial smart rings. The optimal number of turns to maximize the signal-to-noise ratio will vary slightly with diameter, but empirically, we have found that 600 - 800 turns is sufficient for the variety of ring sizes that we tested. Small differences between ring sizes and windings are accounted for in the tracking algorithms.

For the transmitter electronics, a small custom PCB (6.9 mm × 11.4 mm), sits horizontally on top of the 3D printed ring. Figure 6 (right) shows a block diagram of AuraRing's transmitter. The transmitter uses a surface-mounted oscillator (ACZ-32.768) to generate a 32.768 kHz square wave. This frequency was chosen because it is a commonly used frequency for low-frequency clocks on microcontrollers and there is an abundance of integrated chips that produce this frequency. We use a capacitor network to tune the coil's impedance at 32.768 kHz and maximize the transmit power of AuraRing. The series capacitor stores charge that can be drawn through the inductive coil on each cycle of the waveform. This effectively reduces the operating voltage required to generate a given field strength. For a detailed discussion of the effect of these resonant networks on tracking systems, see [22]. The transmitter is powered with two 12 mA h, 1.55 V coin cell batteries with a diameter of 4.8 mm and a height of 2.1 mm.

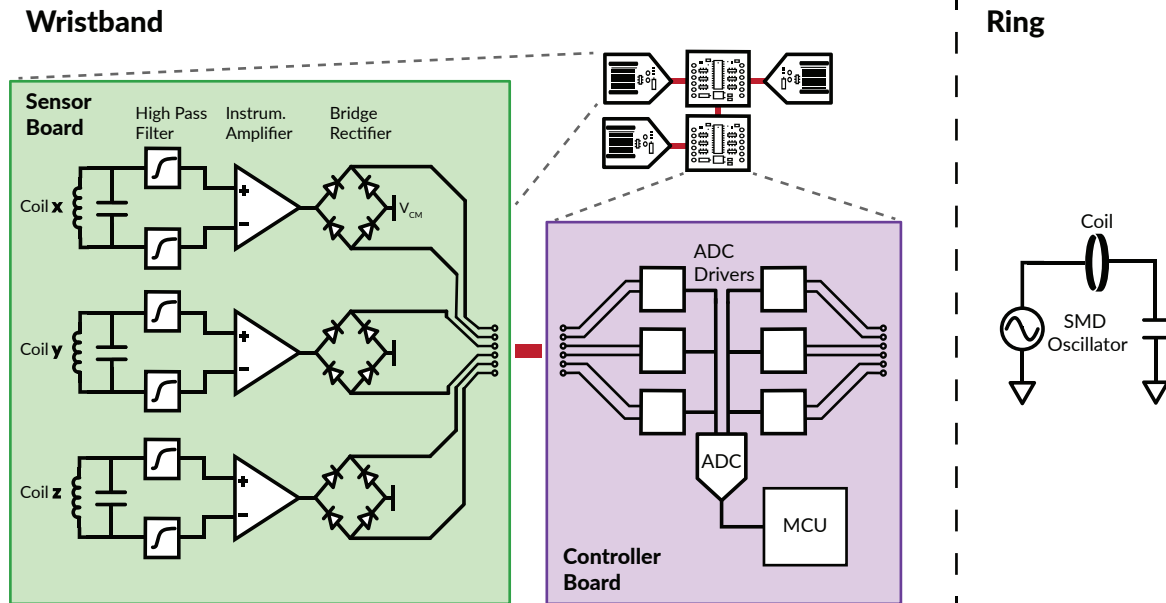


Fig. 6. Block diagram of AuraRing. The ring generates a magnetic field at a particular frequency which is measured by the sensor boards. They send these signals to the controller board where an ADC samples the data and communicates with a host computer using an ultra low power MCU.

4.2 Wristband

The AuraRing wristband consists of three sensors and two controller boards as depicted in Figure 6 (left). At a high level, the sensor boards each measure a magnetic field while the controller boards convert these measurements to digital signals and communicate them to a host computer.

The sensing pipeline is adapted from the signal processing techniques validated for use in electromagnetic tracking applications in Aura [54]. The sensor boards transduce the magnetic field generated by the ring using an off-the-shelf three-axis orthogonal receiver coil (Grupo Premo 3DC15). The signal from each axis is fed to an amplifier (INA826) with a gain of 44 dB. We then use a low-noise and low-voltage drop Schottky diode network (SMS7630) in a full-wave bridge rectifier configuration to demodulate each of the channels. This passive configuration effectively demodulates the field with minimal power consumption and complexity. It should be noted that this method only provides the absolute value of each channel; AuraRing does not know whether each channel is in- or out-of-phase with the transmitter. However, because of the hand's kinematics, most of the channels' signs remain constant, so there is not much information lost. In Section 6, we show that AuraRing can still track without knowing the exact signs of the fields.

These magnitude signals are passed to a controller board with a 10-wire FFC cable. Each controller board supports two sensor boards. By vertically stacking two controller boards within the center of the wristband, AuraRing supports up to four sensors. Based on the analysis in Section 3.3, three coils are sufficient for tracking, so we connect two of the sensors boards to the top controller board and one to the bottom board.

On each of the controller boards, there is an SAR analog-to-digital converter (AD7265) that samples six differential signals simultaneously at 31.25 kHz. Each channel on the controller board has an ADC driver (LTC6363) to achieve high precision, resolution, and throughput. Finally, the sampled data is passed to an ultra-low power

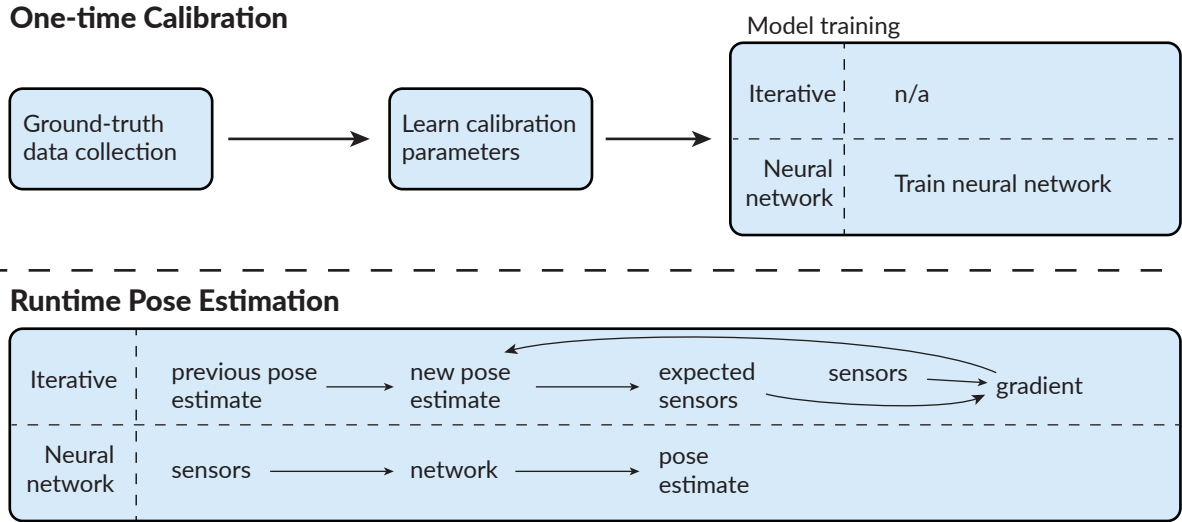


Fig. 7. The AuraRing system needs a one-time factory calibration to match the synthetic data to its measurements. In real-time, the iterative model uses this calibration to refine the pose estimation and the neural network model regresses directly to pose.

MCU (MSP430FR2422) for further processing and communication. Every eight ADC readings, the bottom controller board sends the sampled data to the top controller board where the data is collected and sent to a host computer over USB at 472 kHz. Figure 6 summarizes the analog signal processing of AuraRing.

5 CALIBRATION

AuraRing’s tracking algorithms have, at their core, a physics model, described in Section 3.2. This can be directly used in a parametric model-based tracking algorithm (see Section 6.1) or can be used to generate synthetic data for model training (see Section 6.2). However, before the physics model can accurately describe the AuraRing measurements, we must learn a number of parameters, such as channel gains and precise sensor positions. In a precise manufacturing environment, these parameters can likely be set based on an analysis of the system geometry and electronics. However, in our prototype, due to the tolerances of 3D printed parts and our selection of electronic components, we opt to learn these parameters empirically by collecting and using data from an optical motion capture system. This calibration is a one-time process based on data collected in a controlled environment. After this procedure, AuraRing can be used without any additional training. In the following sections, we describe our data collection setup, the calibration model, and learning procedure. Figure 7 shows a high-level overview of the calibration process and how it relates to the runtime pose estimation task.

5.1 Data Collection Setup

We use a 10-camera¹ optical motion capture system (calibrated accuracy of 0.1 mm) to track the ground truth position and orientation of the wrist and ring. To facilitate this, we place IR retroreflective markers on both devices, as shown in Figure 8. These markers are placed on temporary 3D-printed adapters to ensure they remain

¹OptiTrack Prime 13



Fig. 8. We place retroreflective markers on the ring and wristband to get the ground truth measurement from an optical capture system.

at known locations. Let m be the coordinate system corresponding to the motion capture system, r be the ring's coordinate system, and w be the wristband coordinate system, as defined in Section 3.2. Here, we distinguish between the ring frame (r , used here) and the dipole frame (d , used in the magnetic field calculations). While these two frames are ideally coincident, the magnetic center of the ring may be slightly offset because it is hand-wound around the ring. The motion capture system reports the pose of the wristband (${}^m\mathbf{w}$, ${}^m\mathbf{R}$) and ring (${}^m\mathbf{r}$, ${}^r\mathbf{R}$) in the motion capture coordinate frame at 240 Hz. Software in Python on a PC logs both the motion capture data and AuraRing sensor data to disk for offline analysis.

We first preprocess all of the motion capture data to align the rigid body coordinate frames to the w and r frames defined by the device geometry, as shown in Figure 2. Next, we reconstruct the relative pose of the ring in wrist space by applying another coordinate system transformation.

$${}^w\mathbf{r} = {}^w\mathbf{R} ({}^m\mathbf{r} - {}^m\mathbf{w}) \quad (4)$$

$${}^r\mathbf{R} = {}^r\mathbf{R} \times {}^w\mathbf{R}^T \quad (5)$$

Finally, we synchronize the sensor stream from AuraRing (472 Hz) with the ground truth ring pose stream from motion capture system (240 Hz). Such a synchronization requires the comparison of correlated events in each data stream, but the raw sensor data is uncorrelated with the ground truth pose data. To address this challenge, we use the time-alignment technique presented in Aura [54]. We align the two streams by using the ground truth ring pose as an input to the uncalibrated magnetic field model (Section 3.2) to approximate the magnetic fields at each sensor and comparing these fields to the observed sensor values. Because this model is as yet uncalibrated, this simulated sensor stream does not perfectly match the observed data, but is correlated enough for alignment purposes. We use these signals to achieve alignment at the start and end of the recorded data streams. We then resample the AuraRing signal through interpolation to 240 Hz to achieve frame-by-frame alignment with the ground truth signal. During this process, we drop any frames in which the motion capture system lost track of either the ring or wristband.

5.2 Sensor Model Parameters

The signal processing pipeline in AuraRing transduces the incident magnetic field to a digital value. For a given ring pose, we need to be able to estimate the digital values reported by each sensor. Doing so accurately requires additional calibration parameters that define the *sensor model*, which describes how a given pose manifests as sensor measurements. These parameters model effects like the sensitivity of each coil and the relative positioning

of the sensor coil on the PCB. Altogether, they capture offsets between the motion capture positions and the effective magnetic origins as well as effects of the AuraRing analog signal processing pipeline. These parameters are expected to remain constant throughout the lifetime of the device. Below, we briefly outline these parameters and how they fit into the AuraRing sensor model.

5.2.1 Coordinate System Offsets. Due to manufacturing tolerances, the exact position of each sensor with respect to the wristband coordinate system, ${}^w\mathbf{s}_i$, does not exactly align with the computed values from the CAD design (${}^w\mathbf{s}_{i,CAD}$, ${}^w\mathbf{R}_{i,CAD}$). Since the sensor model estimates the magnetic fields at the sensor positions, it is essential that the sensor pose be as accurate as possible. Consequently, we define offset positions (${}^w\mathbf{s}_{i,offset}$) and orientations ($\mathbf{R}_{i,offset}$) to refine each sensor pose in the wristband frame. These slack terms are expected to be small — on the order of a couple of millimeters or degrees — but they make a significant difference in the tracking performance. The following equations describe how the slack terms are used with the CAD measurements to obtain the exact sensor pose.

$${}^w\mathbf{s}_i = {}^w\mathbf{s}_{i,CAD} + {}^w\mathbf{s}_{i,offset} \quad (6)$$

$${}^w\mathbf{R}_i = {}^w\mathbf{R}_{i,CAD} \times \mathbf{R}_{i,offset} \quad (7)$$

We use a similar technique to define the dipole coordinate frame with respect to the ring coordinate frame, where ${}^r\mathbf{d}$ and ${}^d_r\mathbf{R}$ represent the offset between the r and d frames. Again, this is done to account for the practical side effects of winding our own coils.

$${}^w\mathbf{d} = {}^w\mathbf{r} + {}^w_r\mathbf{R} {}^r\mathbf{d} \quad (8)$$

$${}^d_w\mathbf{R} = {}^d_r\mathbf{R} \times {}^r_w\mathbf{R} \quad (9)$$

Specifically, the unknown parameters are ${}^w\mathbf{s}_{i,offset}$ (3 terms), $\mathbf{R}_{i,offset}$ (4 terms in quaternion form), ${}^r\mathbf{d}$ (3 terms), and ${}^d_w\mathbf{R}$ (4 terms in quaternion form).

5.2.2 Modeling Analog Signal Chain. We then use the model in Section 3.2 to compute ${}^{si}\mathbf{B}_{s_i}$, the magnetic field in each sensor reference frame. However, the sensors and amplitude demodulation pipeline do not represent a perfect measurement of the magnetic field. For one, the rectifier-based demodulation scheme only provides an unsigned estimate of the field strength along each axis. Moreover, each channel has a slightly different gain, due to different sensitivities and manufacturing tolerances of both the sensor coil and amplifiers. We also model the effects of noise and the diode forward voltage drop. Specifically, we estimate the sensor measurement ($x_{i,j}$) as a function of the field (${}^{si}B_{s_i,j}$) and the channel gain ($g_{i,j}$), noise ($n_{i,j}$), and bias ($b_{i,j}$), where $i = \{1, 2, 3\}$ indicates the sensor and $j = \{x, y, z\}$ indicates the axis of a particular sensor. This model is adapted from the calibration model presented and validated in [54].

$$x_{i,j} = \sqrt{(g_{i,j} \times {}^{si}B_{s_i,j})^2 + n_{i,j}^2} - b_{i,j} \quad (10)$$

For a given sensor coil, i , there are 9 signal chain parameters to learn: $g_{i,j}$, $n_{i,j}$, and $b_{i,j}$ for $j = \{x, y, z\}$.

5.3 Learning Sensor Model Parameters

We learn the set of 23 parameters (14 from coordinate system offsets and 9 from the analog signal chain) separately for each sensor, i . To learn these parameters, we collected a dataset that captures a wide range of motion of the ring. One of the authors wore the wristband while using the other hand to move and rotate the ring transmitter freely within in a volume around the hand. During this process, the ring and wrist pose are captured by the motion capture system and aligned as previously described. The data was explicitly collected without wearing the

ring so that this dataset contains 6-DoF motion of the ring. Otherwise, the data would be constrained by the 4-DoF wrist and finger kinematics of a particular user and it may be possible to overfit these parameters to that user.

We took a random sample of 30k frames from this dataset to use for learning and formulated the problem as a non-linear optimization problem, which we solve using Ceres Solver [2]. We learn the 23 parameters for each sensor coil independently. In doing so, the solver seeks to find the parameter set which minimizes the difference between the observed sensor values and the estimated sensor values, computed according to the observed pose and the sensor model. The solver uses the Levenberg-Marquardt trust region algorithm for minimization.

Upon convergence, this results in a set of parameters that can be used to estimate the sensor measurements as a function of pose. Figure 9 shows the correlation between the sensor estimates and actual measurements on this dataset before and after applying the sensor model presented here. Before applying the sensor model, the estimates have a 0.564 Spearman’s rank-order correlation with the actual measurements. After applying the sensor model, the correlation increases to 0.995, validating the effectiveness of this model.

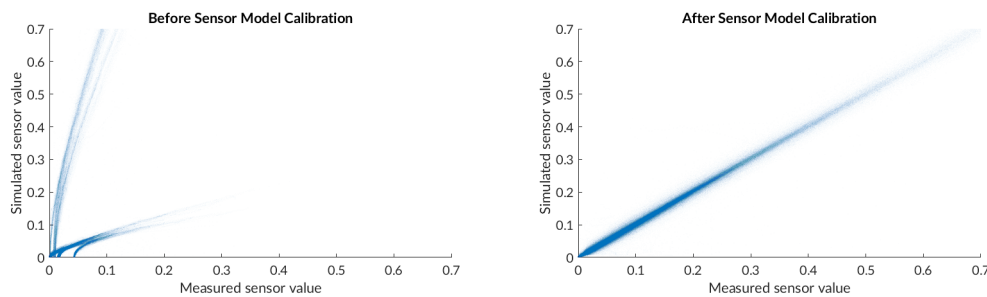


Fig. 9. The one-time factory calibration process is necessary to match the synthetic data to the data measured by AuraRing.

6 TRACKING ALGORITHM

Taken together, the magnetic field model and sensor model represent a forward model of the system—they estimate the sensor values given the ring pose. To track the ring at runtime, we must solve the reverse problem—estimating the ring pose given the sensor values. We implemented two different tracking algorithms to solve this reverse problem and estimate the 5-DoF pose of the ring. The first is an iterative optimization-based solution and the second is a neural network that approximates a closed-form solution to the reverse problem.

6.1 Approach 1: Iterative Model

The iterative model is similar to the method of learning calibration parameters discussed in Section 5.3, but operates on each frame separately. However, instead of estimating the calibration parameters, these remain fixed and the solver estimates the pose of the ring. We use a non-linear optimizer [2] with the Levenberg-Marquardt algorithm to iteratively find the most likely pose. When a new packet of sensor data arrives, the solver minimizes the error between the observed sensor values and the sensor values predicted by the forward model ($x_{i,j}$, Equation 10). It is allowed to run for a maximum of 100 iterations. For the first frame, the initial pose state is set to a default pose with the index finger pointing forward without bending. For subsequent frames, the solver uses the solution to the previous frame as the initial state. Further improvements in speed and accuracy may be possible by using a Kalman filter to proactively estimate the next ring pose.

Because the sensor measurements in the presence of a weak field fundamentally have a lower signal-to-noise ratio (SNR), we do not want these measurements to significantly affect our tracking performance. Moreover, because Equation 10 has a minima when the field is null, there is the potential to get stuck in this minima. To

reduce the impact of these effects, for any of the nine channels in which the measured magnetic field is extremely weak, we simply drop this term from the cost function.

6.2 Approach 2: Neural Network-based Tracking

As an alternative to the iterative model, we also developed closed-form approximations to the reverse problem that are optimized for use on low-power devices. Specifically, we trained a simple neural network to predict both the 3 DoF position and 2 DoF orientation of the ring directly from the magnetic measurements. Notably, we use only synthetically generated data to train the network, eliminating any user or session dependence.

6.2.1 Generating Training Data. Neural networks are particularly sensitive to the quality of the training data. In this tracking problem, insufficient sampling of any portion of the tracking space will result in poor performance. An appropriate neural network approximation to this problem either requires a prohibitively large amount of training data or a smaller but uniformly distributed set of data. To eliminate any dependence on runtime training data and to achieve precise control over the sampling distribution of the training data, we train the network entirely from synthetic data generated by our simulated magnetic and sensor models, after the one-time calibration. This eliminates issues of over-fitting to a particular user's hand or to a particular training session. We randomly generated different ring poses within a volume relative to the wrist that spans possible positions of the ring for most adults. Specifically, assuming the coordinate system defined in Figure 2, the generated data covers a volume defined by $-70 \text{ mm} < X < 90 \text{ mm}$, $-125 \text{ mm} < Y < 60 \text{ mm}$ and $-150 \text{ mm} < Z < -60 \text{ mm}$. We also add a random 3-DoF rotation to each point to complete the dataset of random poses.

We then use the sensor model to estimate the values of AuraRing's sensors at each pose. Since AuraRing uses 3 three-axis receivers and each axis could be in or out of phase with the transmitter, there are $2^9 = 512$ possible combination of phase states for a given frame. However, due to the spatial geometry of our sensors and the kinematic structure of a hand, the majority of these states are not feasible during normal use. For example, because the ring always lies in front of (negative z-direction) the wristband, all of the z-channels of the sensors will have the same phase. In fact, after reviewing the generated data we found that only ten of these 512 combinations are feasible. We drop any data from the generated dataset that does not match one of these ten feasible phase states. Since training uses only simulated data, one could easily change these constraints or even add another state and train a larger network to support different kinds of tracking tasks. After this culling process, the dataset consists of 166,465 points.

6.2.2 Neural Network Training. We use two computationally simple two-layer feed-forward network to regress to a position vector and the 2-DoF orientation of the ring. Both networks have a single hidden layer of 128 nodes to fit a function that maps the nine observed sensor values to a 3-dimensional position vector and to a 3-dimensions direction vector. We use a direction vector to specify orientation in order to remain invariant to the roll of the ring. Training using the synthetic dataset is performed in MATLAB with the Levenberg-Marquardt algorithm. With CPU training on a single core of a Xeon E3-1240 processor, training takes about six hours. Mean training error was 3.06 mm for the position model and 5.45° for the orientation model. Orientation error was calculated by computing the angle between the two direction vectors.

7 SYSTEM EVALUATION

7.1 Tracking Accuracy

7.1.1 User Evaluation Procedure. We evaluate the tracking accuracy of each of these models using data collected from users who we invited to try AuraRing. We do this to provide a realistic estimate of real-world performance under challenging conditions like different hand size, shape, flexibility, slippage of the devices on the hand and finger, and changes in environmental factors. We recruited 14 participants (5 M, 9 F) with different hand sizes



Fig. 10. Data collection setup. IR retroreflective markers are placed on the ring, palm, and wristband to facilitate tracking. The user moves the index finger and wrist while measurements are collected. AuraRing streams data to the PC over a USB connection.

to wear AuraRing while exercising the full range of motion of their wrist and fingers. The data collection was carried out in the same 10-camera motion capture lab used to calibrate the sensor model. The researchers helped the participants put on the wristband and placed the ring on the index finger of the right hand. The average distance between the ring and wristband across all participants was 12.3 cm (min: 10.8 cm, max: 14.3 cm). During operation, the closest distance between the ring and wristband was 8.1 cm and the furthest distance was 15.6 cm.

To ensure no issues related to battery life, the ring was powered with a slightly larger 105 mA h LiPo battery that they held within their hand. As before, markers were placed on an attachment to the ring and wristband to facilitate optical tracking. As showed in Figure 10, we placed additional four markers on the top side of the hand for debugging and visualization purposes. The participants were asked to freely and naturally move their wrist and finger for 10 minutes, while being sure to exercise all possible joint motion. During this time, the ground-truth pose and the magnetic sensors data was recorded by a Python program.

After processing the data, we dropped data from two participants due to poor quality of the optical tracking caused by occlusions. Altogether, this resulted in more than two hours of data consisting of over 1.7 million synchronized data points.

Table 1. Shows the position and orientation error among 12 participants using iterative and neural network models

Mean error (std. dev.)	Iterative Model	Neural Network
X (mm)	1.65 (1.36)	2.85 (2.18)
Y (mm)	3.41 (3.09)	4.18 (2.91)
Z (mm)	1.14 (1.34)	1.80 (2.64)
Euclidean Error (mm)	4.41 (3.05)	6.07 (3.79)
Orientation Error (degrees)	4.65 (3.63)	8.35 (4.72)

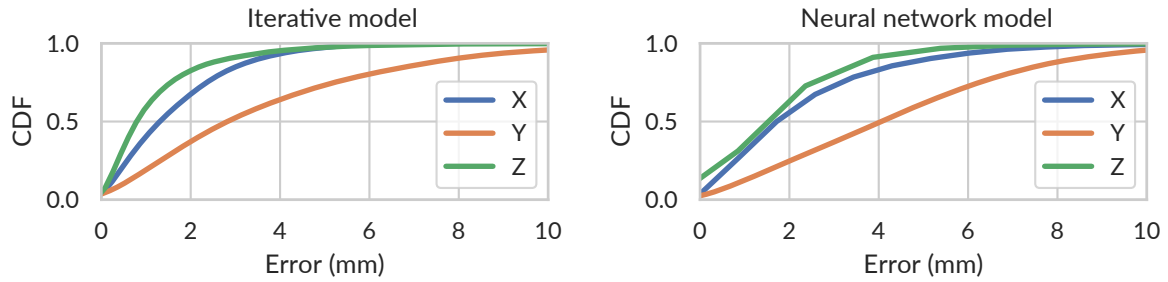


Fig. 11. CDF of 3D position tracking among all participants using the iterative model vs the neural network model.

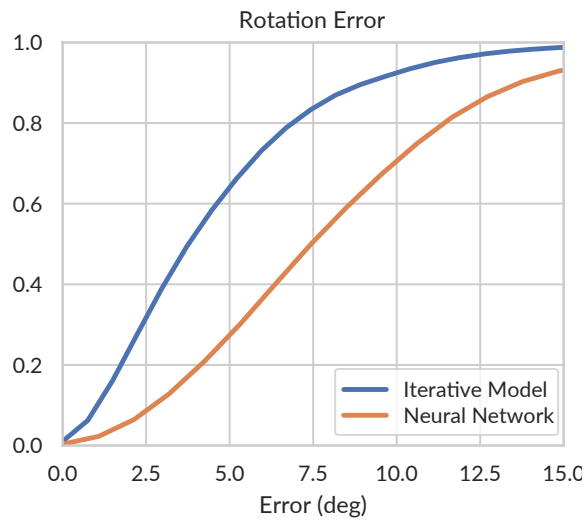


Fig. 12. CDF of orientation tracking among all participants using all models

7.1.2 *Results.* We compare the tracking accuracy for both the iterative and neural network model. Table 1 shows the mean accuracy for the pose of the finger using each algorithm. The full error distribution is shown in the cumulative distribution function (CDF) in Figure 11 that aggregates data across all twelve participants. These results show a mean tracking error of 4.41 mm for the iterative model and 6.07 mm for the neural network model.

For orientation, the iterative model tracks the forward direction of the finger with a mean error of 4.65° and the neural network tracks with a mean error of 8.35°. The full distribution of orientation error for each model is shown in Figure 12.

Tracking performance is better in a neutral pose with performance degrading slightly as the finger moves to the periphery. Figure 13 shows the spatial distribution of positional tracking error on the iterative model projected onto a 2D plane for a representative user. Figure 14 breaks down the error in the iterative model by distance across all users. The model performs best at around 13 cm range. Higher error outside this region can be explained by nonlinearities in the sensing pipeline that are not perfectly captured by our model.

While accuracy is an important measure of tracking performance, the ability to track relative motion is essential if using AuraRing as an input device. Figure 15 shows the ground truth and estimated position over a

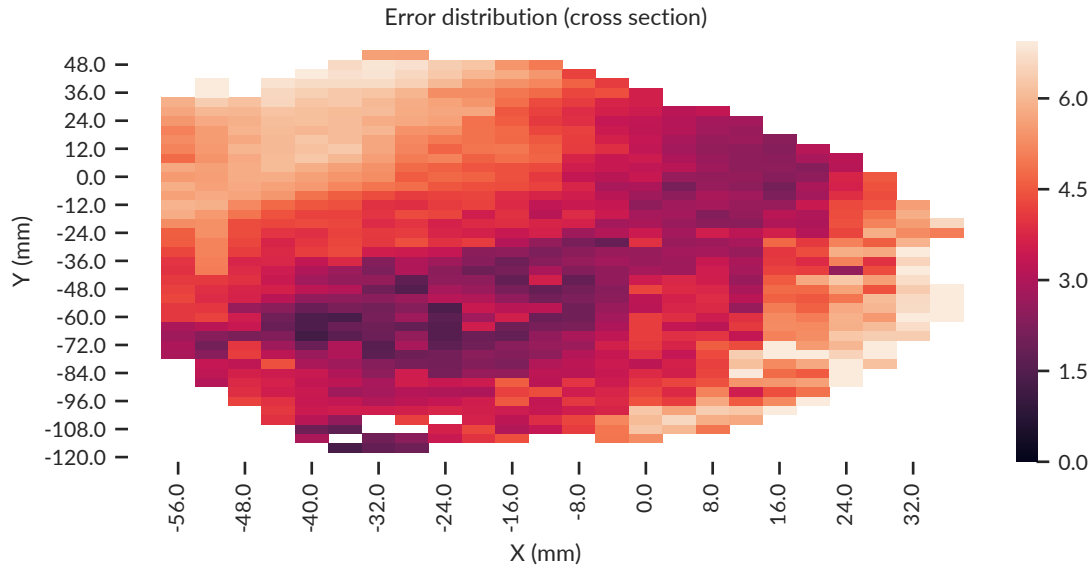


Fig. 13. Heatmap showing spatial distribution of error for a representative user (mean error: 4.36 mm) for iterative model

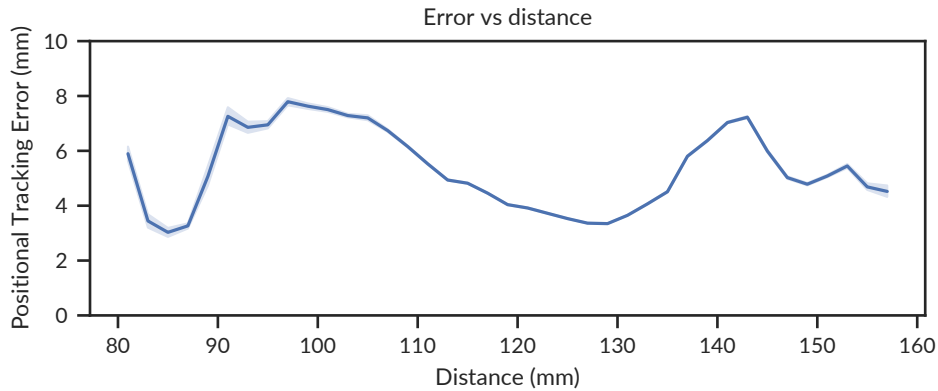


Fig. 14. Euclidian tracking error as a function of distance across all participants for iterative model

representative few seconds of two representative sample traces. The sample trace on the left, has a below average mean error on the iterative model of 2.56 mm. The trace on the right performs worse at 4.99 mm. Note that even in cases where the error is relatively high, the relative motion still tracks the ground truth motion. These traces do not have any additional Kalman filtering applied to them.

To better understand the dynamics of each model, Figure 16 shows a highly zoomed in trace of the x-direction only for a representative 200 ms window. The dark lines indicate estimates that have been smoothed with a Kalman filter. The lighter lines represent the raw estimates from each model. This shows that even in the case of a static offset in tracking, the relative pose tracks well, even over timescales of tens of milliseconds. This pattern holds for the neural network model as well.

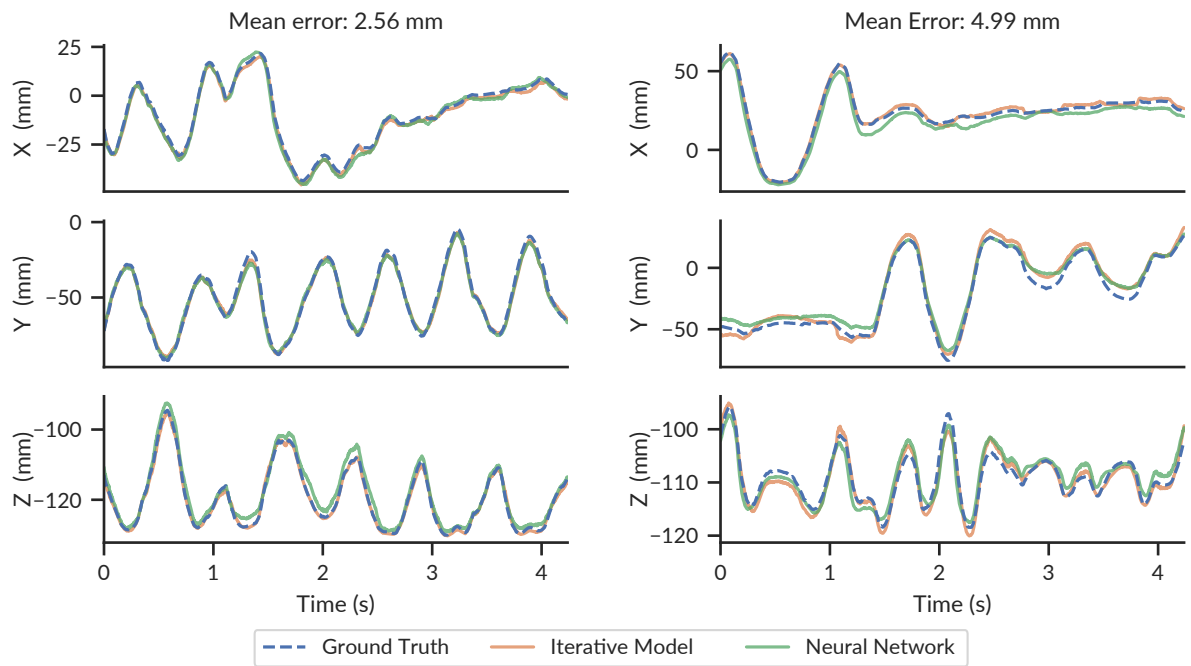


Fig. 15. A representative few seconds of 3D positional tracking for two of the participants. While the tracking error is relatively higher for the one on the right, the relative motion still tracks the ground truth motion.

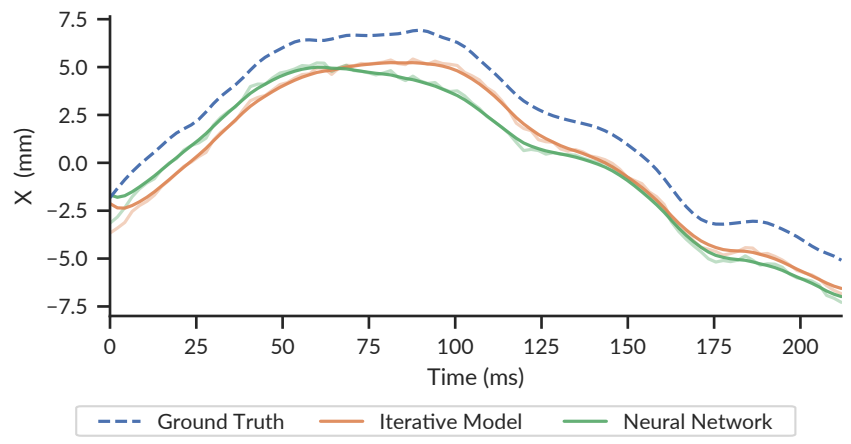


Fig. 16. A zoomed in trace for the x-direction. AuraRing leverages a Kalman filter to smooth out the estimated position. Even when the neural network has a static offset, the relative motion is preserved.

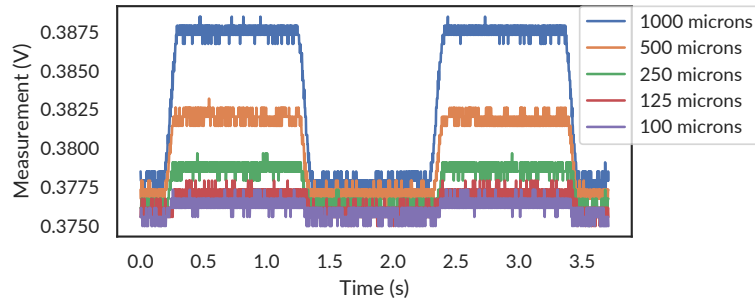


Fig. 17. The AuraRing hardware is sensitive to 100 microns of movement. A single channel of one of the sensors depicted as the transmitter is moved by a motorized linear stage.

7.2 Resolution

Resolution is an important characterization for a sensor system that quantifies the smallest detectable change in the measure of interest. The use of high-precision electromagnetic sensors represents a significant advantage for AuraRing over other wearable sensing systems because of its ability to capture small and subtle interactions.

We used a motorized linear stage² to quantify the resolution of the AuraRing hardware. The stage is software-controllable and has a repeatability of 10 μm and a step size of 0.2 μm . We affix the ring to the stage and place the wristband 125 mm away, a typical operating distance during normal use. The devices were oriented such that most of the magnetic flux is oriented in the z-direction of the wristband. We programmed the stage to move back and forth (in the z-direction) and variable step sizes ranging from 100 μm to 1 mm. Figure 17 shows the values measured in one of the sensor coils during this procedure. No filtering was applied to this data. From this figure, one can observe that a step size of 1 mm is clearly visible. As the step size decreases to 100 μm , the difference in sensor readings approaches the size of a single bit of the ADC.

We note that because the device is capable of sampling at speeds much faster than a typical user interface would require, the resolution could likely be significantly improved through filtering. We also note that because we do not have a ground truth measure of the AC magnetic field strength, the resolution here depends on the specific position at which it is measured. Nonetheless, this is a representative example that illustrates the sensitivity of the hardware platform.

7.3 Power

We measured the power consumption of both the ring and wristband of AuraRing using a USB oscilloscope to measure the voltage drop across a series resistor of values 9.8 Ω and 109.5 Ω for the ring and wristband respectively. The ring consumes only 715 μA of current (2.34 mW) and the wristband consumes 22.2 mA (73.3 mW). Two 12 mA h batteries that fit comfortably on the ring PCB allow the ring to operate continuously for about 17 hours. A 2 W h battery would allow the wristband to continuously operate for more than a full day. In practice, such a system could have a sleep functionality so that the transmitter and processing circuitry do not need to be on when not in use.

7.4 Speed and Compute

Although the analysis presented in this work was performed offline, the algorithms used for pose estimation were designed with real-time operation in mind. The iterative approach performs the best, but requires the most

²PI VT-80

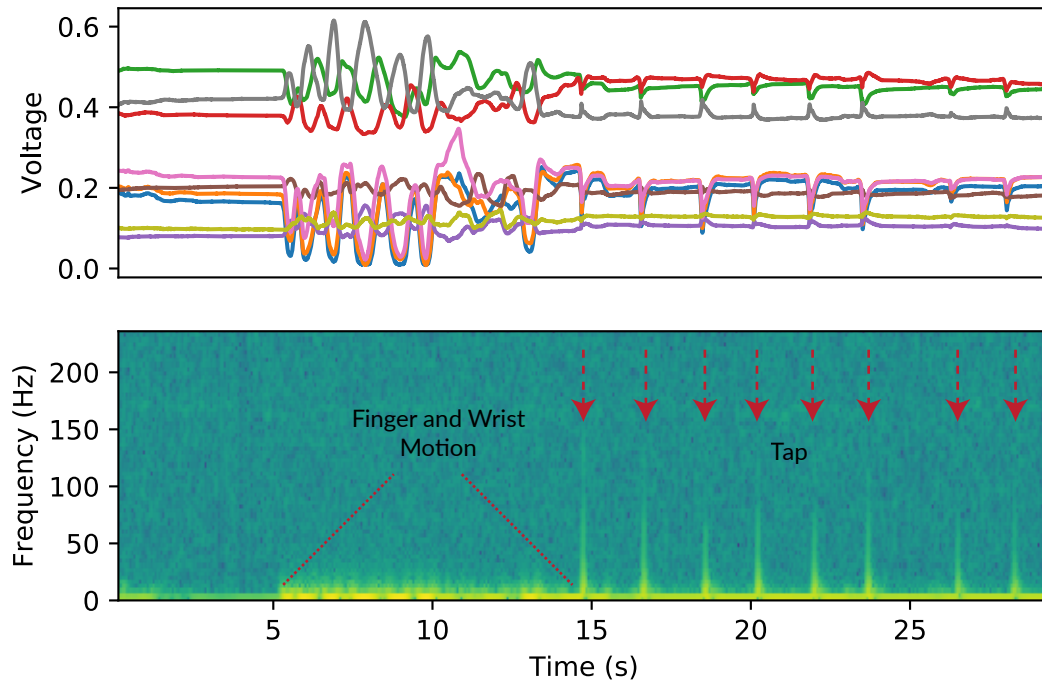


Fig. 18. AuraRing is capable of measuring high-speed events such as taps. A user performs multiple taps after moving their finger in the air. (Top): nine raw sensor measurements. (Bottom): Spectrogram of the recorded data.

compute power. However, despite the iterative nature of the algorithm, it easily exceeds realtime speeds. When fed each data frame sequentially, the algorithm operates at speeds exceeding 1 kHz on a single core of a Xeon E3-1240 processor. We anticipate that, with some care, it is possible to port this algorithm to a mobile processor.

However, in scenarios where compute is at a premium, such as on a mixed-reality HMD, we designed the neural network approach for maximum efficiency. The network contains only a single layer with 128 hidden nodes. Runtime position and orientation estimation consists of just two matrix multiplications for each (9×128 and 128×3).

8 ADDITIONAL FUNCTIONALITY

Having the ability to track one's finger precisely without line-of-sight enables a wide range of applications. However, we believe that the speed and precision which AuraRing's magnetic tracking enables unlocks additional functionality not commonly found in wearable sensing systems. In this section we discuss and demonstrate a few additional features that AuraRing can enable.

8.1 Tap Detection

Visions of free-hand interaction techniques in AR and VR commonly include in-air taps and gestures. However whether you are clicking in an app on your AR glasses or drawing in a VR game, the sensation of touch is one of

the critical factors for an immersive experience. The ability to robustly detect taps on environmental and body surfaces enables new kinds of always-available ambient interfaces [17, 57]. AuraRing helps enable this future by providing not only an estimate of finger position, but a high-speed robust signal which can be used to detect taps.

With a data rate of 472 Hz and a sensor bandwidth much higher than this, AuraRing is capable of measuring high speed events. To demonstrate this, Figure 18 shows a series of taps of varying intensities on a tabletop surface after a period of freely moving the finger and wrist in space. The lower portion of the figure shows a spectrogram with a window size of 128. While hand and finger motion contain mostly low frequency content, taps are immediately distinguishable due to their broadband spectrum and appear to contain content up to about 150 Hz.

8.2 Free-form Drawing

To demonstrate that AuraRing is useful for much more than just gesture recognition, we show a few example traces of handwriting reconstruction using AuraRing. We consider two types of use cases. For use with a mixed reality HMD, we anticipate the use of wrist-tracking using fiducial markers embedded in the wristband. While one could use the wrist position as a virtual "pen", we argue that the dynamics of the wrist and finger joints are crucial to enabling a compelling experience. In Figure 19, we show two examples of writing the word "hello" in the air; one with large movement over tens of centimeters (left) and another that was "written" on a notebook held in the opposing hand spanning just a couple of centimeters (right). The top row shows the result if one were to use just the wrist position; in this case, the wrist pose was captured from the motion capture system. On large motions, wrist position is a reasonable proxy that might be useful for gesture recognition, but not for precise input. For smaller motions the wrist position results in a poor quality signal. However, as shown in the bottom row, combining the estimate of finger position from AuraRing and wrist position from the motion capture device unlocks new and subtle in-air interactions. In other use cases, the wrist may not be tracked, such as with interaction on a smartwatch. In these cases, AuraRing is still capable of providing an accurate reconstruction of relative fingertip position, which is still useful for handwriting tasks. Figure 1 (left) shows an example of a handwriting trace reconstructed without any optical motion capture system. AuraRing results in a significantly more useful signal. With appropriate visual feedback, we anticipate the performance to be even better.

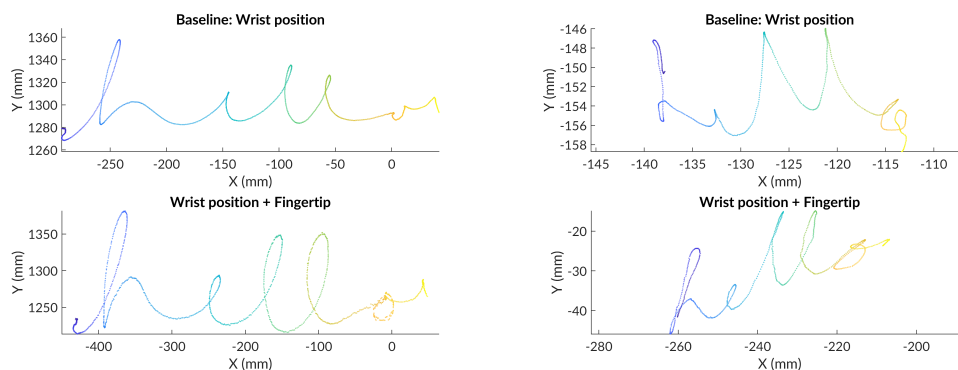


Fig. 19. Handwriting examples using wrist-only motion from motion capture (top) and wrist motion + AuraRing (bottom). The left example shows large hand motion. The right example show small writing on a handheld object.



Fig. 20. The ring pose can be used to drive an inverse kinematics model of the hand, as shown here.

8.3 Inverse Kinematics

Fundamentally, AuraRing tracks the pose of the ring with respect to the wristband. In the evaluation, we demonstrated tracking accuracy, which is the most essential measure of performance. However, since users will wear the ring on the index finger, we can use the tracking data to infer the pose of the hand. Specifically, we can use inverse kinematics to estimate the two wrist joint angles (radiocarpal joint) and two metacarpophalangeal (MCP) angles. This process requires knowledge of two bone lengths in the hand as well as where the wristband is placed on the wrist. Let ${}^a v_{offset}$ be the vector between wrist joint and where the wristband sits on the wrist, b_{met} be the distance between the wrist and MCP joint, and b_{prox} be the distance between the MCP joint and the ring along the proximal phalanx. These distances can either be prespecified or learned automatically as the user moves their hand. As before, let w be the wristband frame and r be the ring frame. We define m to be the frame corresponding to the metacarpal bone, or the body of hand and a to be the frame corresponding to the arm. Furthermore, let ${}^a_w \mathbf{R}$, ${}^m_a \mathbf{R}$, and ${}^r_m \mathbf{R}$ be the rotation from wristband to the arm (wristband placement), arm to the metacarpal (wrist joint), and metacarpal to the proximal phalanx or ring frame (MCP joint), respectively. As shown in the Figure 2, the z-direction is in the direction along the finger; therefore, ${}^r \mathbf{b}_{prox}$ and ${}^m \mathbf{b}_{met}$ represent the bone length vectors which are in the z-direction. We can compute the position of the ring with respect to the wristband (${}^w \mathbf{r}$) using the following equation:

$${}^w \mathbf{r} = {}^w \mathbf{R} ({}^a v_{offset} + {}^a_m \mathbf{R} ({}^m \mathbf{b}_{met} + {}^m_r \mathbf{R} ({}^r \mathbf{b}_{prox}))) \quad (11)$$

By fixing the offsets and bone lengths (${}^a v_{offset}$, ${}^m \mathbf{b}_{met}$, and ${}^r \mathbf{b}_{prox}$) as well as the wristband rotation (${}^a_w \mathbf{R}$), we are left with just the wrist (radiocarpal) and finger (MCP) joints to solve for. We parameterize these with two degrees of freedom each (yaw and pitch) and solve for them using a second-stage optimization on top of the tracking problem. Using Ceres, we find the four joint angles which best explain the ring pose estimate.

9 DISCUSSION

In this work, we demonstrated AuraRing, a wearable device that enables precise tracking of the pose of a smart ring with respect to the wristband. The use of short-range electromagnetic tracking offers unparalleled precision while minimizing the effects of environmental interference. We have proposed two methods for tracking. For more accurate tracking, we use an iterative model that achieves a position accuracy of 4.4 mm and a 2-DoF mean orientation accuracy of 4.65°. In mobile scenarios where computation power is at a premium, we propose a relatively small neural network model with only one hidden layer. Using this approach AuraRing is able to achieve an accuracy of 6 mm across all users.

We envision AuraRing's use either with or without a head-mounted display. For mixed reality scenarios, head-mounted cameras are becoming increasingly capable of tracking the hands and fingers, but doing so comes

at a significant power and compute cost. Tracking infrared fiducial markers in a wristband is a much simpler task. However, in cases where full five-finger tracking is desired, AuraRing can serve as a robust prior to constrain the search space for a traditional hand-tracking algorithm. For interaction with other wearable devices, AuraRing can be used as an indirect input device.

The use of a physics and sensor model is a significant advantage of our tracking algorithm, compared to other data-driven methods. It allows simulation and experimentation to optimize system configuration and decouples model training from user evaluation. That said, AuraRing does still require the use of a one-time factory calibration. For the prototype presented in this work, such a calibration is essential, due to the manufacturing tolerances of the device assembly. However, it is possible that for a mass-produced device, the tolerances can be made tight enough such that a single model would suffice for all units.

Although we intend for the factory calibration to be used across all sessions, we also created a variant of the iterative tracking model that refines the calibration parameters based on two minutes of data from that session. This accounts for drift in parameters like the noise in the analog signal chain, which can be impacted by environmental factors like temperature. We found that tweaking the calibration model using some per-session data can reduce the tracking error to 1.5 mm. We expect that with more attention paid to analog stability, the global error will approach the per-session error. Another promising approach is migrating to digital processing for demodulation. This could enable reconstruction of both the magnitude and phase of the signals. We leave such explorations to future work.

Among related work in sensor-based tracking of the fingers, AuraRing is most similar to Finexus [8]. In AuraRing, we prioritized form-factor and designed the system from the ground up with wearability in mind—both in the design of the ring-worn transmitter and the wrist-based sensors. AuraRing uses significantly less power (2.3 mW on the finger), uses an untethered ring, and estimates 2-DoF rotation in addition to position. In terms of accuracy, AuraRing’s 1.5 mm single-session accuracy is comparable to that reported in the single-session evaluation of Finexus. Moreover, the AuraRing accuracy holds at typical finger-wrist distances, which exceed the operating range of Finexus. Compared to SkinTrack, which was shown to be able to resolve 2D touch locations with a mean error of 7.6 mm, AuraRing tracks with a mean error of 4.4 mm in 5-DoF.

Smart rings are an attractive form-factor for always-available subtle input [4, 10, 11, 15, 24, 35, 58]. However, since all of these methods require sensing on the ring, they have to communicate the data from the ring which prohibits the ring to be a self contained, wearable device. For example, a commonly available smart ring with an integrated inertial measurement unit would have to sample and stream data at tens of hertz over an RF link, which is not feasible. Instead, such devices rely on gesture recognition and stream only sparse discrete events. However, by moving the sensing components from the ring to the wrist, AuraRing can use a slimmer ring design with minimal power consumption and enable high-speed, real-time tracking. AuraRing also differs in that it tracks the absolute 5-DoF pose of the finger and can be used for more than just 2D input on a surface or just as a symbolic text entry device.

With some modifications, AuraRing can support tracking of multiple rings at the same time for multi-finger tracking. Currently the wristband is tuned to the transmitter frequency, but by tuning each ring to different frequencies, AuraRing could time multiplex between the ring’s frequencies and measure the resulting fields. The maximum distance between the wristband and the ring at which AuraRing can still measure changes in the magnetic field is 30 cm. Therefore, for multiple users in the same environment, there is likely little that needs to be done. However, if users wish to operate multiple devices in close proximity, different frequencies can be used.

Like all electromagnetic tracking systems, AuraRing’s performance will degrade in the close proximity to metallic, particularly ferromagnetic, objects. Unlike solutions like Polhemus [41], the AuraRing transmitter and receiver are in relative close proximity, which significantly reduces the scope of possible interference sources. To quantify the effects of large metallic objects on AuraRing, we measured the effect of two commonly used devices (i.e. a smartphone and a laptop) that are likely to be in close proximity to the AuraRing during operation. We

observed no effects on the received signals as long as the device had a distance of at least 15 cm to the wristband and ring.

AuraRing performance could further be improved by additional optimization of the sensor coil positions on the wristband. In general, the performance will improve as they are more spread out. Since we envisioned the ring to be worn on the index finger which is closer to the inside of the hand, we placed two sensors on the left side of the wristband, assuming right-handed use. AuraRing’s hardware has the ability to support four sensor boards without modification of the electronics. For additional performance or for left-handed use, one could install another sensor board to the right side of the wristband.

A challenge in the design of any smart ring is sizing it for an appropriate fit across users. For the purposes of this study, we made the ring larger than average and used tape to wrap around the finger to ensure a snug fit. A more robust design might use several fixed size coils (e.g. small, medium, large) with replaceable insets in standard ring sizes.

In this work, we have placed the ring on the base segment of the finger (proximal phalanx), which is where rings are typically worn. As a result, our system is insensitive to motion in distal and intermediate phalanges. Future work can enable full finger tracking by placing proximity sensors on the ring to track the relative motion of the distal and intermediate phalanges, as was shown in LightRing [24]. Such an extension of AuraRing might modulate the transmitter signal with this additional information to convey the data back to the wristband without an additional RF link.

Although this work focuses on the use of a ring to track the finger, AuraRing could also be used as a generic tracking platform for handheld objects. For example, by putting a coil around a stencil or pen, the object could be made trackable with respect to the wrist. Pen input could be automatically digitized, a toy could be automatically turned into a gaming controller, or a toothbrush can monitor how someone is brushing their teeth.

Future work can also explore the use of a completely battery-free ring. The AuraRing system uses a transmitter on the ring and measure the resulting fields on the wristband. An alternative method of tracking could be to use AuraRing’s wristband’s coils as both the transmitter and receiver. In this topology, the ring is a tuned LC network that will change the measurements on the wristband based on its pose.

To make AuraRing available to the community, we have open-sourced the hardware designs and algorithms used in this work.³

10 CONCLUSION

In this work, we present AuraRing, a wearable ring and wristband that enables precise, subtle and accurate finger tracking. Using minimal, low-power electronics on the ring, AuraRing can operate for about a day on self-contained batteries. We presented two methods for tracking, a neural network-based approach and an iterative model. AuraRing only needs a one-time factory calibration process to match its synthetic data to sensor measurements and can track with a mean error of 4.4 mm. For additional performance, recalibration can be used to achieve a mean positional error of 1.5 mm.

ACKNOWLEDGMENTS

This work was supported by the UW Reality Lab, Facebook, Google, and Huawei. We also thank the Global Innovation Exchange for access to their motion capture systems as well as Tianke Li, Alvin Cao, and Ishan Chatterjee for their assistance.

³<https://github.com/ubicomplab/AuraRing>

REFERENCES

- [1] 5DT. [n.d.]. 5DT Data Glove Ultra Series. <http://www.5dt.com/downloads/dataglove/ultra/5DTDataGloveUltraDatashet.pdf>. Accessed: 2019-05-09.
- [2] Sameer Agarwal, Keir Mierle, and Others. [n.d.]. Ceres Solver. <http://ceres-solver.org>.
- [3] Christoph Amma, Marcus Georgi, and Tanja Schultz. 2012. Airwriting: Hands-free mobile text input by spotting and continuous recognition of 3D-space handwriting with inertial sensors. In *2012 16th International Symposium on Wearable Computers*. IEEE, 52–59.
- [4] Daniel Ashbrook, Patrick Baudisch, and Sean White. 2011. NENYA: subtle and eyes-free mobile input with a magnetically-tracked finger ring. In *Proceedings of the SIGCHI Conference on Human Factors in Computing Systems*. ACM, 2043–2046.
- [5] Liwei Chan, Yi-Ling Chen, Chi-Hao Hsieh, Rong-Hao Liang, and Bing-Yu Chen. 2015. Cyclopsring: Enabling whole-hand and context-aware interactions through a fisheye ring. In *Proceedings of the 28th Annual ACM Symposium on User Interface Software & Technology*. ACM, 549–556.
- [6] Liwei Chan, Rong-Hao Liang, Ming-Chang Tsai, Kai-Yin Cheng, Chao-Huai Su, Mike Y Chen, Wen-Huang Cheng, and Bing-Yu Chen. 2013. FingerPad: private and subtle interaction using fingertips. In *Proceedings of the 26th annual ACM symposium on User interface software and technology*. ACM, 255–260.
- [7] Ke-Yu Chen, Kent Lyons, Sean White, and Shwetak Patel. 2013. uTrack: 3D input using two magnetic sensors. In *Proceedings of the 26th annual ACM symposium on User interface software and technology*. ACM, 237–244.
- [8] Ke-Yu Chen, Shwetak N Patel, and Sean Keller. 2016. Finexus: Tracking precise motions of multiple fingertips using magnetic sensing. In *Proceedings of the 2016 CHI Conference on Human Factors in Computing Systems*. ACM, 1504–1514.
- [9] Marvin P Fried, Jonathan Kleeffeld, Harsha Gopal, Edward Reardon, Bryan T Ho, and Frederick A Kuhn. 1997. Image-guided endoscopic surgery: results of accuracy and performance in a multicenter clinical study using an electromagnetic tracking system. *The Laryngoscope* 107, 5 (1997), 594–601.
- [10] Masaaki Fukumoto and Yasuhito Suenaga. 1994. “FingerRing”: A Full-time Wearable Interface. In *Conference Companion on Human Factors in Computing Systems (CHI '94)*. ACM, New York, NY, USA, 81–82. <https://doi.org/10.1145/259963.260056>
- [11] Masaaki Fukumoto and Yoshinobu Tonomura. 1997. “Body Coupled FingerRing”: Wireless Wearable Keyboard. In *Proceedings of the ACM SIGCHI Conference on Human Factors in Computing Systems (CHI '97)*. ACM, New York, NY, USA, 147–154. <https://doi.org/10.1145/258549.258636>
- [12] X. Ge, D. Lai, X. Wu, and Z. Fang. 2009. A novel non-model-based 6-DOF electromagnetic tracking method using non-iterative algorithm. In *2009 Annual International Conference of the IEEE Engineering in Medicine and Biology Society*. 5144–5117. <https://doi.org/10.1109/IEMBS.2009.5332723>
- [13] Peregrine Glove. [n.d.]. Peregrine Glove ST. <https://peregrineglove.com/products/peregrine-glove-st-full-kit-w-pod>. Accessed: 2019-05-09.
- [14] Jun Gong, Yang Zhang, Xia Zhou, and Xing-Dong Yang. 2017. Pyro: Thumb-tip gesture recognition using pyroelectric infrared sensing. In *Proceedings of the 30th Annual ACM Symposium on User Interface Software and Technology*. ACM, 553–563.
- [15] Aakar Gupta, Cheng Ji, Hui-Shyong Yeo, Aaron Quigley, and Daniel Vogel. 2019. RotoSwype: Word-Gesture Typing Using a Ring. In *Proceedings of the 2019 CHI Conference on Human Factors in Computing Systems (CHI '19)*. ACM, New York, NY, USA, Article 14, 12 pages. <https://doi.org/10.1145/3290605.3300244>
- [16] Chris Harrison and Scott E Hudson. 2009. Abracadabra: wireless, high-precision, and unpowered finger input for very small mobile devices. In *Proceedings of the 22nd annual ACM symposium on User interface software and technology*. ACM, 121–124.
- [17] Chris Harrison, Desney Tan, and Dan Morris. 2010. Skinput: appropriating the body as an input surface. In *Proceedings of the SIGCHI conference on human factors in computing systems*. ACM, 453–462.
- [18] Yi-Ta Hsieh, Antti Jylhä, Valeria Orso, Luciano Gamberini, and Giulio Jacucci. 2016. Designing a Willing-to-Use-in-Public Hand Gestural Interaction Technique for Smart Glasses. In *Proceedings of the 2016 CHI Conference on Human Factors in Computing Systems (CHI '16)*. ACM, New York, NY, USA, 4203–4215. <https://doi.org/10.1145/2858036.2858436>
- [19] Da-Yuan Huang, Liwei Chan, Shuo Yang, Fan Wang, Rong-Hao Liang, De-Nian Yang, Yi-Ping Hung, and Bing-Yu Chen. 2016. DigitSpace: Designing Thumb-to-Fingers Touch Interfaces for One-Handed and Eyes-Free Interactions. In *Proceedings of the 2016 CHI Conference on Human Factors in Computing Systems*. ACM, 1526–1537.
- [20] Jiawei Huang, Tsuyoshi Mori, Kazuki Takashima, Shuichiro Hashi, and Yoshifumi Kitamura. 2015. IM6D: Magnetic Tracking System with 6-DOF Passive Markers for Dexterous 3D Interaction and Motion. *ACM Trans. Graph.* 34, 6, Article 217 (Oct. 2015), 10 pages. <https://doi.org/10.1145/2816795.2818135>
- [21] Yasha Iravantchi, Yang Zhang, Evi Bernitsas, Mayank Goel, and Chris Harrison. 2019. Interferi: Gesture Sensing Using On-Body Acoustic Interferometry. In *Proceedings of the 2019 CHI Conference on Human Factors in Computing Systems (CHI '19)*. ACM, New York, NY, USA, Article 276, 13 pages. <https://doi.org/10.1145/3290605.3300506>
- [22] Mohd Noor Islam and Andrew J Fleming. 2018. Resonance-Enhanced Coupling for Range Extension of Electromagnetic Tracking Systems. *IEEE Transactions on Magnetics* 54, 4 (2018), 1–9.

- [23] Seungwoo Je, Brendan Rooney, Liwei Chan, and Andrea Bianchi. 2017. tactoRing: A Skin-Drag Discrete Display. In *Proceedings of the 2017 CHI Conference on Human Factors in Computing Systems (CHI '17)*. ACM, New York, NY, USA, 3106–3114. <https://doi.org/10.1145/3025453.3025703>
- [24] Wolf Kienzle and Ken Hinckley. 2014. LightRing: Always-available 2D Input on Any Surface. In *Proceedings of the 27th Annual ACM Symposium on User Interface Software and Technology (UIST '14)*. ACM, New York, NY, USA, 157–160. <https://doi.org/10.1145/2642918.2647376>
- [25] David Kim, Otmar Hilliges, Shahram Izadi, Alex D Butler, Jiawen Chen, Iason Oikonomidis, and Patrick Olivier. 2012. Digits: freehand 3D interactions anywhere using a wrist-worn gloveless sensor. In *Proceedings of the 25th annual ACM symposium on User interface software and technology*. ACM, 167–176.
- [26] Wooyoung Kim, Jihoon Song, and Frank C Park. 2018. Closed-form position and orientation estimation for a three-axis electromagnetic tracking system. *IEEE Transactions on Industrial Electronics* 65, 5 (2018), 4331–4337.
- [27] Volodymyr V Kindratenko. 2000. A survey of electromagnetic position tracker calibration techniques. *Virtual Reality* 5, 3 (2000), 169–182.
- [28] Volodymyr V Kindratenko and William R Sherman. 2005. Neural network-based calibration of electromagnetic tracking systems. *Virtual Reality* 9, 1 (2005), 70–78.
- [29] Jack B Kuipers. 1980. SPASYN—an electromagnetic relative position and orientation tracking system. *IEEE Transactions on Instrumentation and Measurement* 29, 4 (1980), 462–466.
- [30] Katja M Langen, Twyla R Willoughby, Sanford L Meeks, Anand Santhanam, Alexis Cunningham, Lisa Levine, and Patrick A Kupelian. 2008. Observations on real-time prostate gland motion using electromagnetic tracking. *International Journal of Radiation Oncology* Biology* Physics* 71, 4 (2008), 1084–1090.
- [31] Mingyu Liu, Mathieu Nancel, and Daniel Vogel. 2015. Gunslinger: Subtle arms-down mid-air interaction. In *Proceedings of the 28th Annual ACM Symposium on User Interface Software & Technology*. ACM, 63–71.
- [32] Kent Lyons. 2016. 2D input for virtual reality enclosures with magnetic field sensing. In *Proceedings of the 2016 ACM International Symposium on Wearable Computers*. ACM, 176–183.
- [33] Jess McIntosh, Paul Strohmeier, Jarrod Knibbe, Sebastian Boring, and Kasper Hornbæk. 2019. Magnetips: Combining Fingertip Tracking and Haptic Feedback for Around-Device Interaction. In *Proceedings of the 2019 CHI Conference on Human Factors in Computing Systems (CHI '19)*. ACM, New York, NY, USA, Article 408, 12 pages. <https://doi.org/10.1145/3290605.3300638>
- [34] CGM Meskers, HM Vermeulen, JH De Groot, FCT Van der Helm, and PM Rozing. 1998. 3D shoulder position measurements using a six-degree-of-freedom electromagnetic tracking device. *Clinical biomechanics* 13, 4 (1998), 280–292.
- [35] Suranga Nanayakkara, Roy Shilkrot, Kian Peen Yeo, and Pattie Maes. 2013. EyeRing: a finger-worn input device for seamless interactions with our surroundings. In *Proceedings of the 4th Augmented Human International Conference*. ACM, 13–20.
- [36] Rajalakshmi Nandakumar, Vikram Iyer, Desney Tan, and Shyamnath Gollakota. 2016. Fingerio: Using active sonar for fine-grained finger tracking. In *Proceedings of the 2016 CHI Conference on Human Factors in Computing Systems*. ACM, 1515–1525.
- [37] NDI. [n.d.]. Medical Aurora - Medical. <https://www.ndigital.com/medical/products/aurora/>. Accessed: 2019-05-09.
- [38] Valter Pasku, Alessio De Angelis, Guido De Angelis, Darmindra D Arumugam, Marco Dionigi, Paolo Carbone, Antonio Moschitta, and David S Ricketts. 2017. Magnetic field-based positioning systems. *IEEE Communications Surveys & Tutorials* 19, 3 (2017), 2003–2017.
- [39] D Perie, AJ Tate, PL Cheng, and GA Dumas. 2002. Evaluation and calibration of an electromagnetic tracking device for biomechanical analysis of lifting tasks. *Journal of biomechanics* 35, 2 (2002), 293–297.
- [40] G. Pirkel, K. Stockinger, K. Kunze, and P. Lukowicz. 2008. Adapting magnetic resonant coupling based relative positioning technology for wearable activity recognition. In *2008 12th IEEE International Symposium on Wearable Computers*. 47–54. <https://doi.org/10.1109/ISWC.2008.4911584>
- [41] Polhemus. [n.d.]. Polhemus G4. <https://polhemus.com/motion-tracking/all-trackers/g4>. Accessed: 2018-12-11.
- [42] Z.B. Popović and B.D. Popović. 2000. *Introductory Electromagnetics*. Prentice Hall. <https://books.google.com/books?id=-S9HAQAAIAAJ>
- [43] Frederick H Raab, Ernest B Blood, Terry O Steiner, and Herbert R Jones. 1979. Magnetic position and orientation tracking system. *IEEE Transactions on Aerospace and Electronic systems* 5 (1979), 709–718.
- [44] Gabriel Reyes, Jason Wu, Nikita Juneja, Maxim Goldshtein, W. Keith Edwards, Gregory D. Abowd, and Thad Starner. 2018. SynchroWatch: One-Handed Synchronous Smartwatch Gestures Using Correlation and Magnetic Sensing. *Proc. ACM Interact. Mob. Wearable Ubiquitous Technol.* 1, 4, Article 158 (Jan. 2018), 26 pages. <https://doi.org/10.1145/3161162>
- [45] Thijs Roumen, Simon T. Perrault, and Shengdong Zhao. 2015. NotiRing: A Comparative Study of Notification Channels for Wearable Interactive Rings. In *Proceedings of the 33rd Annual ACM Conference on Human Factors in Computing Systems (CHI '15)*. ACM, New York, NY, USA, 2497–2500. <https://doi.org/10.1145/2702123.2702350>
- [46] S. Song, C. Hu, B. Li, X. Li, and M. Q. Meng. 2013. An Electromagnetic Localization and Orientation Method Based on Rotating Magnetic Dipole. *IEEE Transactions on Magnetics* 49, 3 (March 2013), 1274–1277. <https://doi.org/10.1109/TMAG.2012.2211375>
- [47] S. Song, H. Ren, and H. Yu. 2014. An Improved Magnetic Tracking Method Using Rotating Uniaxial Coil With Sparse Points and Closed Form Analytic Solution. *IEEE Sensors Journal* 14, 10 (Oct 2014), 3585–3592. <https://doi.org/10.1109/JSEN.2014.2329186>

- [48] CyberGlove Systems. [n.d.]. CyberGlove II. <http://www.cyberglovesystems.com/cyberglove-ii>. Accessed: 2019-05-09.
- [49] Jonathan Taylor, Lucas Bordeaux, Thomas Cashman, Bob Corish, Cem Keskin, Toby Sharp, Eduardo Soto, David Sweeney, Julien Valentin, Benjamin Luff, et al. 2016. Efficient and precise interactive hand tracking through joint, continuous optimization of pose and correspondences. *ACM Transactions on Graphics (TOG)* 35, 4 (2016), 143.
- [50] Hoang Truong, Shuo Zhang, Ufuk Muncuk, Phuc Nguyen, Nam Bui, Anh Nguyen, Qin Lv, Kaushik Chowdhury, Thang Dinh, and Tam Vu. 2018. CapBand: Battery-free Successive Capacitance Sensing Wristband for Hand Gesture Recognition. In *Proceedings of the 16th ACM Conference on Embedded Networked Sensor Systems (SenSys '18)*. ACM, New York, NY, USA, 54–67. <https://doi.org/10.1145/3274783.3274854>
- [51] Robert Y Wang and Jovan Popović. 2009. Real-time hand-tracking with a color glove. *ACM transactions on graphics (TOG)* 28, 3 (2009), 63.
- [52] Saiwen Wang, Jie Song, Jaime Lien, Ivan Poupyrev, and Otmar Hilliges. 2016. Interacting with soli: Exploring fine-grained dynamic gesture recognition in the radio-frequency spectrum. In *Proceedings of the 29th Annual Symposium on User Interface Software and Technology*. ACM, 851–860.
- [53] Eric Whitmire, Mohit Jain, Divye Jain, Greg Nelson, Ravi Karkar, Shwetak Patel, and Mayank Goel. 2017. Digitouch: Reconfigurable thumb-to-finger input and text entry on head-mounted displays. *Proceedings of the ACM on Interactive, Mobile, Wearable and Ubiquitous Technologies* 1, 3 (2017), 113.
- [54] Eric Whitmire, Farshid Salemi Parizi, and Shwetak Patel. 2019. Aura: Inside-out Electromagnetic Controller Tracking. In *Proceedings of the 17th Annual International Conference on Mobile Systems, Applications, and Services (MobiSys '19)*. ACM, New York, NY, USA, 300–312. <https://doi.org/10.1145/3307334.3326090>
- [55] Eric Whitmire, Laura Trutoiu, Robert Cavin, David Perek, Brian Scally, James Phillips, and Shwetak Patel. 2016. EyeContact: scleral coil eye tracking for virtual reality. In *Proceedings of the 2016 ACM International Symposium on Wearable Computers*. ACM, 184–191.
- [56] Guofang Xiao, Ester Bonmati, Stephen Thompson, Joe Evans, John Hipwell, Daniil Nikitichev, Kurinchi Gurusamy, Sébastien Ourselin, David J Hawkes, Brian Davidson, et al. 2018. Electromagnetic tracking in image-guided laparoscopic surgery: Comparison with optical tracking and feasibility study of a combined laparoscope and laparoscopic ultrasound system. *Medical physics* 45, 11 (2018), 5094–5104.
- [57] Robert Xiao, Julia Schwarz, Nick Throm, Andrew D Wilson, and Hrvoje Benko. 2018. MRTouch: Adding Touch Input to Head-Mounted Mixed Reality. *IEEE transactions on visualization and computer graphics* 24, 4 (2018), 1653–1660.
- [58] Xing-Dong Yang, Tovi Grossman, Daniel Wigdor, and George Fitzmaurice. 2012. Magic finger: always-available input through finger instrumentation. In *Proceedings of the 25th annual ACM symposium on User interface software and technology*. ACM, 147–156.
- [59] Hui-Shyong Yeo, Juyoung Lee, Hyung-il Kim, Aakar Gupta, Andrea Bianchi, Daniel Vogel, Hideki Koike, Woontack Woo, and Aaron Quigley. 2019. WRIST: Watch-Ring Interaction and Sensing Technique for Wrist Gestures and Macro-Micro Pointing. In *Proceedings of the 21st International Conference on Human-Computer Interaction with Mobile Devices and Services (MobileHCI '19)*. ACM, New York, NY, USA, Article 19, 15 pages. <https://doi.org/10.1145/3338286.3340130>
- [60] Sang Ho Yoon, Ke Huo, Vinh P. Nguyen, and Karthik Ramani. 2015. TIMMi: Finger-worn Textile Input Device with Multimodal Sensing in Mobile Interaction. In *Proceedings of the Ninth International Conference on Tangible, Embedded, and Embodied Interaction (TEI '15)*. ACM, New York, NY, USA, 269–272. <https://doi.org/10.1145/2677199.2680560>
- [61] Sang Ho Yoon, Ke Huo, and Karthik Ramani. 2014. Plex: Finger-worn Textile Sensor for Mobile Interaction During Activities. In *Proceedings of the 2014 ACM International Joint Conference on Pervasive and Ubiquitous Computing: Adjunct Publication (UbiComp '14 Adjunct)*. ACM, New York, NY, USA, 191–194. <https://doi.org/10.1145/2638728.2638746>
- [62] Yang Zhang and Chris Harrison. 2015. Tomo: Wearable, low-cost electrical impedance tomography for hand gesture recognition. In *Proceedings of the 28th Annual ACM Symposium on User Interface Software & Technology*. ACM, 167–173.
- [63] Yang Zhang, Robert Xiao, and Chris Harrison. 2016. Advancing hand gesture recognition with high resolution electrical impedance tomography. In *Proceedings of the 29th Annual Symposium on User Interface Software and Technology*. ACM, 843–850.
- [64] Yang Zhang, Junhan Zhou, Gierad Laput, and Chris Harrison. 2016. Skintrack: Using the body as an electrical waveguide for continuous finger tracking on the skin. In *Proceedings of the 2016 CHI Conference on Human Factors in Computing Systems*. ACM, 1491–1503.